DESIGN AND CHARACTERIZATION OF NOVEL PIEZOCERAMIC C-BLOCK ACTUATORS FOR A BALANCED ACTIVE FLAP SYSTEM

Final Report

Grant # DAAH04-96-1-0186

Joseph W. Clement* and Diann Brei†, The University of Michigan

Andrew J. Moskalik‡, US EPA National Vehicle and Fuel Emissions Laboratory

Ron Barrett§, Auburn University

---

* Graduate Student, Department of Mechanical Engineering and Applied Mechanics, The University of Michigan, Ann Arbor, Michigan 48109-2125

† Assistant Professor, Department of Mechanical Engineering and Applied Mechanics, The University of Michigan, Ann Arbor, Michigan 48109-2125

‡ Mechanical Research Engineer, Advanced Technology Division, The US EPA National Vehicle and Fuel Emissions Laboratory, Ann Arbor MI 48105

§ Associate Professor, Department of Aerospace Engineering, Auburn University, Auburn University, AL 36849-5338

REPORT DOCUMENTATION PAGE

Form Approved
OMB NO. 0704-0188

1. AGENCY USE ONLY (Leave Blank)	2. REPORT DATE	3. REPORT TYPE AND DATES COVERED
	31 October 2000	Final January 1996- July 2000

4. TITLE AND SUBTITLE
Design and Characterization of Novel Piezoceramic C-block Actuators for a Balanced Active Flap System

5. FUNDING NUMBERS
DAAH04-96-1-0186

6. AUTHOR(S)
Dr. Diann Brei, Dr. Ron Barrett, Dr. Andrew Moskalik, Joseph Clement

7. PERFORMING ORGANIZATION NAME(S) AND ADDRESS(ES)
The University of Michigan, 2250 G.G. Brown, Ann Arbor, MI 48109-2125

Auburn University, 211 Aerospace Engineering Bldg., Auburn, AL 36849-5338

8. PERFORMING ORGANIZATION REPORT NUMBER

9. SPONSORING / MONITORING AGENCY NAME(S) AND ADDRESS(ES)

U. S. Army Research Office
P.O. Box 12211
Research Triangle Park, NC 27709-2211

10. SPONSORING / MONITORING AGENCY REPORT NUMBER

ARO 34775.5-EG

11. SUPPLEMENTARY NOTES
The views, opinions and/or findings contained in this report are those of the author(s) and should not be construed as an official Department of the Army position, policy or decision, unless so designated by other documentation.

12 a. DISTRIBUTION / AVAILABILITY STATEMENT	12 b. DISTRIBUTION CODE
Approved for public release; distribution unlimited.	

13. ABSTRACT (Maximum 200 words)
In this research, a high authority piezoceramic actuation technology was developed to drive an active flap system with less sensitivity to gust loads and little to no degradation in performance with increasing rotor speed. This research effort took a new approach to active flap control through the usage of C-blocks, a promising actuator architecture with midrange performance, high efficiency, and a tailorable architecture. When applied to rotorcraft, this system has potential to reduce vibration levels and yield better handling and overall performance. This system is also beneficial for fixed wing applications such as munitions guidance and UAV control. The two primary tasks of this research were a) to design and characterize piezoceramic C-block actuators and b) to develop and wind tunnel test an aerodynamically and mass balanced active rotor blade flap incorporating C-block actuators. Through analytical modeling and experimental validation over a broad design range, this research has established the foundation to apply this actuation technology to a wide range of applications. As a demonstration of the actuator's high authority and the benefits of impedance tailoring, the actuators were integrated into a NACA 0012 airfoil with a 10% flap and generated high flap deflections with no significant sensitivity to airspeed.

14. SUBJECT TERMS	15. NUMBER OF PAGES
Active Rotor Blade Flaps Piezoceramic C-block Actuators Vibration Control	59
	16. PRICE CODE

17. SECURITY CLASSIFICATION OR REPORT	18. SECURITY CLASSIFICATION ON THIS PAGE	19. SECURITY CLASSIFICATION OF ABSTRACT	20. LIMITATION OF ABSTRACT
UNCLASSIFIED	UNCLASSIFIED	UNCLASSIFIED	UL

FOREWORD

In this research, a high authority piezoceramic actuation technology was developed to drive an active flap system with less sensitivity to gust loads and little to no degradation in performance with increasing rotor speed. This research effort took a new approach to active flap control through the usage of C-blocks, a promising actuator architecture with midrange performance, high efficiency, and a tailorable architecture. When applied to rotorcraft, this system has potential to reduce vibration levels and yield better handling and overall performance. This system is also beneficial for fixed wing applications such as munitions guidance and UAV control. The two primary tasks of this research were a) to design and characterize piezoceramic C-block actuators and b) to develop and wind tunnel test an aerodynamically and mass balanced active rotor blade flap incorporating C-block actuators. Through analytical modeling and experimental validation over a broad design range, this research has established the foundation to apply this actuation technology to a wide range of applications. As a demonstration of the actuator's high authority and the benefits of impedance tailoring, the actuators were integrated into a NACA 0012 airfoil with a 10% flap and generated high flap deflections with no significant sensitivity to airspeed.

TABLE OF CONTENTS

Page Number

LIST OF ILLUSTRATIONS

Page Number

1.0 INTRODUCTION

1.1 Motivation

One of the main problems affecting modern helicopter performance is the large vibratory load generated as the rotors travel through an extremely complex flow field. The primary source of the vibrations is the differential in air speeds encountered by the retreating and advancing blades. Because the air speed is much lower over the retreating blade, an increase in the retreating blade's pitch is required to maintain lateral stability. As a result of the pitching action, a N/rev load is transmitted to the fuselage for a N-bladed helicopter. In addition to the physical discomfort experienced by the passengers, the vibrations create excessive levels of noise, cause premature replacement of the rotor blades, and reduce payload capabilities.

For over a decade, researchers have known about the benefits of using Higher Harmonic Control (HHC) for suppression of vibration and enhancement of performance in rotorcraft. Several series of investigations on MD-500 series helicopters at McDonnell Douglas Helicopter Company throughout the late 1980's showed that manipulation of the blades at rates in excess of 3/rev could ameliorate many of the adverse effects of shed vortices and retreating blade stall in high speed flight. As a result, vibration levels were significantly reduced and dash speed was increased. However, there were several major difficulties, in particular, the large power consumption of the actuators, overall system complexity and thermal issues. Because the possibility for significant performance enhancement through HHC was clearly demonstrated, researchers have been pursuing this line of research for the past decade, resulting in studies that revealed that HHC vibration control could be further improved if each blade could be manipulated independently.

The concept of Individual Blade Control (IBC) should theoretically produce even greater performance gains and vibration level reduction. However, in addition to the power consumption and complexity difficulties, the IBC system must be decoupled even further from the fixed frame than an HHC system. To accomplish this, investigators have been experimenting with novel ways of integrating actuator mechanisms into the blades themselves. Since 1989, investigators, such as Spangler and Hall (1990), Barrett (1990a,b,c), Samak and Chopra (1993, 1994), Prechtl and Hall (1999, 1997), Fulton and Ormiston (1998, 1997), Duvernier et al., 2000, Hall et al., 2000; Lee

and Chopra, 2000, 1999, Giurgiutiu, Rogers, and Rusovici (1996), Koratkar and Chopra (2000, 1997), Straub and Merkley (1997), and Rusovici and Cudney, (1997) have invented systems which directly change the shape of the blade or move aerodynamic surfaces on the blade. Later studies targeting missile controls, such as active fins for high-speed missiles (August and Joshi, 1996), the torque-plate concept (Barrett 1993a,b,c, 1994b,c), and the Flexspar configuration (Barrett, 1994a; Barrett, Gross & Brozoski, 1995) can be tailored to rotorcraft applications. Although these missile designs have been specifically created for high-speed flight at high angles of attack without consideration for the high fatigue environment as found in rotorcraft, expansions of the torque-plate and Flexspar designs are currently underway and include modifications to minimize high strain fatigue effects.

For IBC to be successful, proper actuation is critical. Most actuation approaches investigated for active flap control are based on piezoelectric actuation. Conventional actuators such as electric motors and hydraulic systems are relatively inefficient, contain a large number of parts, and are difficult to scale for smaller systems such as UAV or small munitions guidance (Giurgiutiu, 2000). In contrast, piezoelectric actuators are lightweight, more efficient, have a much larger bandwidth, and are easily scaled for smaller applications such as munitions guidance. While there are other smart material actuation methods that provide high energy densities, piezoelectrics are still the most common because magnetostrictive actuators utilize heavy magnetic coils, electrostrictive actuators require strong biasing electric fields to offset its one-directional operation and shape memory alloy actuators operate with much lower bandwidths.

Although piezoelectric actuators are a promising technology for active flap control, developing a system architecture to deliver the required force and deflection while fitting within the space available is challenging. Piezoelectric material, although relatively light and power-dense (Baz and Poh, 1988; Damjanovic and Newnham, 1992), delivers limited direct strain; thus, the material must be built into a strain-amplified architecture to be effective in this application. There exists three primary methods of strain amplification: external, such as leveraged stacks, internal, such as benders, and frequency. Frequency leveraged actuators, such as the Inchworm (Burleigh, 1998), are well suited to positioning applications due to their high precision; however they suffer from a reduced frequency response at high displacements limiting, their effectiveness for vibration suppression applications. Utilizing leveraged stack actuators for active flap actuation has been heavily researched (Hall et al., 2000; Lee and Chopra, 2000, 1999; Prechtl and

Hall, 1999, 1997; Spencer and Chopra, 1996) due the ability to position the stack near the wing's center of gravity and because of the stack uses the higher energy dense "33" mode (~2.5 times more energy than the "31" mode). However, achieving the large deflection amplification ratios necessary to provide sufficient deflections for active flap control without incurring high transmission losses can be difficult (Paine, and Chaudhry, 1996). However, several clever amplification methods have been developed since the beginning of this research which minimize the energy loss in the external lever (Hall et al., 2000, Lee and Chopra, 2000). While benders typically utilize the lower energy "31" mode, they have the distinct advantage of not requiring a separate leveraging system which reduces weight and leads to a very mass efficient architecture and therefore have been incorporated into many active flap systems (Fulton and Ormiston, 1997; Ben-Zeev and Chopra, 1996; Spangler and Hall, 1990). Simple straight benders tend to be highly compliant, allowing for great displacement, but at the cost of force (Near, 1996), creating an inefficient impedance mismatch to the active flap application (Guiguirtui et al., 1995). Therefore, current research has modified the straight bender, forming tapered benders to improve the efficiency of the actuator while better matching the actuator's stiffness to the flap application (Koratkar and Chopra, 2000, 1997; Hall and Prechtl, 1996). Less conventional actuators, such as RAINBOWs (Haertling, 1994), THUNDERs (Face, 1997), and Moonies (Suguwara et al., 1993) are both difficult to fit in the available space and suffer from transmission losses inherent in the architecture (Kugel et al., 1997; Near, 1996).

1.2 Research Problem Statement and Goals

The problem studied in this research is the development of a new piezoceramic actuation technology with the authority to drive an active flap system which will be less sensitive to gust loads and will experience little to no degradation in performance with increasing rotor speed. Such a system can be applied to rotorcraft leading to reduced vibration levels, better handling and overall improved performance. To accomplish this goal, this research effort took a new approach to active flap actuation – C-blocks. The goal was to exploit the tailorable C-block actuation architecture to create an internally amplified piezoceramic actuator that allows for very large aerodynamically balanced flap deflections (up to 10° pp) while maintaining an adequate frequency response of at least 4/rev.

The two primary tasks of this research were a) to design and characterize C-block piezoceramic actuators having capabilities required by rotorcraft applications and b) to develop and wind tunnel test an aerodynamically and mass balanced active rotor blade flap using piezoceramic C-block actuators. Piezoceramic C-blocks were successfully analytically modeled, fabricated and tested within a NACA 0012 airfoil demonstrating high flap deflections (> 15° pp) with no significant degradation in airspeed or sensitivity to gust loads. The results of the two main tasks leading to this major accomplishment are summarized in the following sections: *2.0 Piezoceramic C-block Actuator Development* and *3.0 Active Flap System Demonstration.*

2.0 PIEZOCERAMIC C-BLOCK ACTUATOR DEVELOPMENT

For active flaps to be effective, actuation is critical. There are several issues that must be addressed for proper actuation:

- The actuator must be matched to the application. Guiguirtui et al. (1995) showed that the proportion of energy from the actuator available for external work is maximized when the stiffnesses of the driving actuator and the external system are matched (Figure 1).
- The actuation system (actuator and any necessary leverage system) must fit within the constrained volume. Applications like the rotor blade smart flap, where the available volume for the actuators is both limited in volume and shape, require specially shaped actuators.
- The actuation system must be mass efficient.
- The actuation system must have sufficient bandwidth for flight control and/or vibration control.

This research utilized a relatively new class of piezoelectric actuators, C-blocks, to address these issues. The C-block is an internally amplified building block architecture which allows for the design of actuator meeting a broad range of application requirements without necessitating inefficient external amplification mechanisms (Figure 2). Individual C-blocks are semicircular

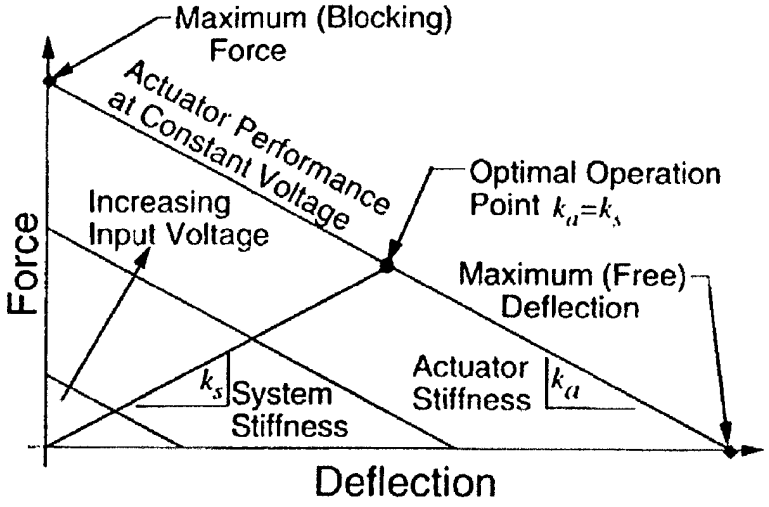

Figure 1. Force-Deflection Model for a Generic Piezoelectric Actuator. This shows the interrelationship among voltage input, force output and deflection output. The optimal operation point is located where the stiffnesses of the actuator and system are matched.

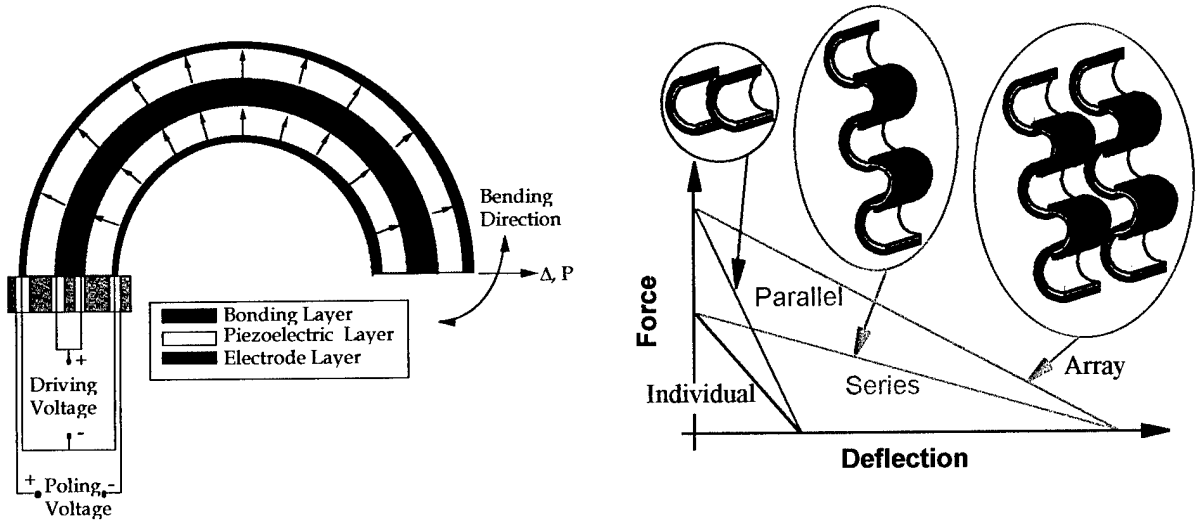

a) Individual C-block **b) C-block Architectures**

Figure 2. C-block Actuator Design and Performance Tailorability The individual C-block actuator is a building block that can be used to construct distributed arrays, enhancing the architecture performance. **a)** The individual C-block is a semicircular bender constructed of piezoelectric material poled radially. **b)** The individual C-block can be combined into serial architectures for deflection enhancement, parallel architectures for force enhancement, or distributed architectures for force and deflection enhancement, and stiffness/impedance matching.

multilayered piezoelectric benders which flex when a voltage is applied across the thickness. The flexing occurs because the active piezoelectric layers are poled in the radial direction and laid up with inert layers to create a bending moment when energized. Research on individual C-blocks (Moskalik and Brei, 1997b) has demonstrated that this architecture produces 2.67 times the force of a comparable straight bender with 40.5% of the deflection, thus overcoming the force limitation of the straight bender while providing two orders of magnitude more deflection of stack actuators. The C-block produces 8% more work than a straight bender constructed from the same volume of material which is significant considering that straight benders are very efficient compared to other internally leveraged architectures such as Rainbows, Crescent and Thunders (Kugel, Chandran, and Cross, 1997).

The main advantage to the C-block architecture is its ability to be used like a building block to construct distributed actuation arrays consisting of number of individual C-blocks to further improve force and deflection (Figure 2b). Since this is a direct extension of the architecture, C-blocks do not experience the transmission losses that can plague frequency and externally leveraged architectures by as much as a factor of three to five (Paine and Chaudhry, 1996). The series and parallel array configuration parameters give engineers two more design freedoms in

addition to the geometric and material parameters that are available in other architectures. This provides a large number of feasible discrete C-block array architectures making it possible to design the actuator directly to the application for optimal stiffness, force, deflection, and bandwidth.

2.1 C-Block Performance Modeling

Research on curved beams has been undertaken since the mid nineteenth century (Love, 1944; Hoppe, 1871). Unfortunately, even today, there is little previous research on serial arrays of curved, piezoelectric laminated beams such as the C-block. The only serial curved beams investigated have been simple elastic suspensions (Shoup, 1971, 1972; Shoup and Simmonds, 1977), which were neither laminate nor piezoelectric, and were constructed in a simple series of two. Other researchers have previously analyzed curved composite beams (Larson and Vinson, 1993b; Qatu, 1993) or shells (Larson and Vinson, 1993a), but these researchers have not combined dynamic analysis, piezoelectric terms, and, more importantly, array configurations. As such, there were no predictive models for C-blocks at the onset of this research effort. Over the course of this investigation, models to predict the static and dynamic performance were derived from fundamental mechanics for both individual C-blocks (Moskalik and Brei, 1997a, 1997b) and C-block arrays (Moskalik and Brei, 1999a, 1999b). Since there is not one comprehensive paper that details the full performance and experimental characterization of the C-block architecture, a summary is given in this report for the model development and design of experiments. This work lays the foundation for the application of this new actuation technology to any application, including active rotor blade flaps.

2.1.1 Equations of Motion and Boundary Conditions

The C-block array was modeled as an array of identical thin, individual C-blocks, having n in series and m in parallel (Figure 3). To account for the system that the C-block array will be actuating, a tip mass and a static force were placed at the free end. The force, F_{tot}, and tip mass, $\mu nm\rho\pi R_n$, can be divided evenly amongst each series in the array (F_y and $\mu n\rho\pi R_n$). Internal damping in the array was modeled as structural damping as discussed in Meirovitch (1967).

The equations of motion and associated boundary conditions for the generic C-block array were derived using Hamilton's principle and including the piezoelectric terms in the internal strain

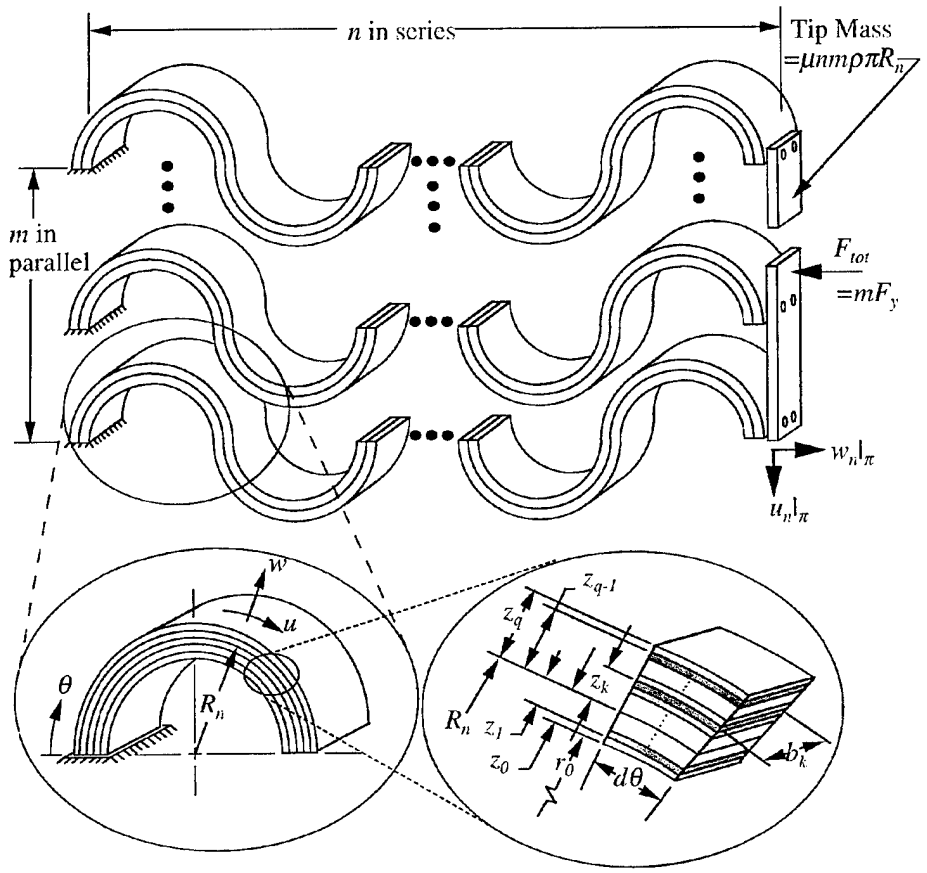

Figure 3. Geometric Notation for a Generic Array of C-blocks A generic array of C-blocks contains *m* sets of C-blocks in parallel and *n* sets of C-blocks in series. Each individual C-block has identical geometric and material parameters, and a tip mass and applied force are distributed evenly among the parallel elements.

energy. These equations are uncoupled in the parallel direction, simplifying the equations for a C-block array to that of a single C-block series, with each C-block in the series having the same equations of motion,

$$\left(\frac{1}{\chi}+1\right)u_{k,\theta\theta}+\frac{1}{\chi}w_{k,\theta}-w_{k,\theta\theta\theta}+\frac{\gamma}{\Omega}\left[\left(\frac{1}{\chi}+1\right)u_{k,\theta\theta}+\frac{1}{\chi}w_{k,\theta}-w_{k,\theta\theta\theta}\right]=\frac{R_n^4}{D}\rho u_{k,tt} \quad (1)$$

$$u_{k,\theta\theta\theta}-\frac{1}{\chi}u_{k,\theta}-\frac{1}{\chi}w-w_{k,\theta\theta\theta\theta}+\frac{\gamma}{\Omega}\left[u_{k,\theta\theta\theta}-\frac{1}{\chi}u_{k,\theta}-\frac{1}{\chi}w-w_{k,\theta\theta\theta\theta}\right]=\frac{R_n^4}{D}\rho w_{k,tt}+\frac{N^P R_n^3}{D}+\frac{\gamma N_{,t}^P R_n^3}{\Omega D}.$$

There are three distinct sets of boundary conditions: 1) at the base ($\theta = 0$) of the first C-block, the displacements, *u* and *w*, and the slope, φ, are zero, 2) at the (*n* - 1) boundaries between

adjacent C-blocks, six physical quantities (i.e., the displacements, u and w, slope, φ, moment, M, shear, V, and normal force, N) match and 3) at the tip of the last (nth) C-block ($\theta = \pi$), the moment, M, shear, V, and normal force, N, are all zero,

$$M_n\big|_\pi = \frac{D}{R_n^2}\left[\left(-w_{n,\theta\theta} + u_{n,\theta} + \frac{M^P R_n^2}{D}\right) + \frac{\gamma}{\Omega}\left(-w_{n,\theta\theta} + u_{n,\theta} + \frac{M_{,t}^P R_n^2}{D}\right)\right]_\pi = 0$$

$$V_n\big|_\pi = \frac{D}{R_n^3}\left[\left(-w_{n,\theta\theta\theta} + u_{n,\theta\theta}\right) + \frac{\gamma}{\Omega}\left(-w_{n,\theta\theta\theta} + u_{n,\theta\theta}\right) - \mu n\pi\lambda_i^2 w + \frac{F_y R_n^3}{D}\right]_\pi = 0 \quad (2)$$

$$N_n\big|_\pi = \frac{D}{R_n^3}\left[\left(u_{n,\theta} + w_n + \frac{N^P \chi R_n^3}{D}\right) + \frac{\gamma}{\Omega}\left(u_{n,\theta} + w_n + \frac{N^P \chi R_n^3}{D}\right) - \mu n\chi\pi\lambda_i^2 u\right]_\pi = 0.$$

These boundary conditions include the forcing functions: piezoelectric force and moment, N^P and M^P, the tip force, F_y and nondimensional tip mass, μ. The n sets of equations of motion (Eq. 1) and $6n$ boundary conditions completely describe the behavior of the serial C-block.

2.1.2 *Static Force-Deflection Model*

The quasi-static force-deflection model was derived from the equation of motion and boundary conditions by removing the time-dependent terms and solving the resulting simplified equations (Moskalik and Brei, 1997b, 1999a). The resulting models relate the deflection at the tip, (u_n and w_n), to the loading, (M^P and F_y). The model for the entire array can be written by summing the forces for each the parallel elements. For the longitudinal (w) direction which would be used in actuation, the final model is

$$F_{tot} = mF_y = \frac{4mM^P}{\pi R_n} - \frac{2w_n mD}{\pi n R_n^3}. \quad (3)$$

From this model, the blocked force is derived by setting $w_n = 0$, and the free deflection is derived by setting $F_y = 0$.

2.1.3 *Dynamic Frequency-Amplitude Model*

The modeling of the dynamic behavior of any serial laminated beam is complex. Therefore, the more advanced transfer matrix method (Pestel and Leckie, 1964) was employed to derive the

dynamic frequency-amplitude model for piezoceramic arrays (Moskalik and Brei, 1999b). This method uses the equations of motion to derive the transfer matrix $[U]$, which relates the vector of state variables, $\{z\} = \{u\ -w\ \varphi\ M\ V\ N\}^T$ evaluated at the tip of an element to the state vector evaluated at the base,

$$\{z\}|_{tip} = [U]\{z\}|_{base}. \tag{4}$$

Elements connected in series, like the C-block, can be easily modeled by multiplying the transfer matrices for each adjacent element to form a single matrix for the entire series. The advantage of this method is that a large number of equations of motion can be simplified into a single matrix equation.

To formulate all the required transfer matrices for a C-block actuation system, the transfer matrix, $[U_i]$, for an individual C-block was derived from the equations of motion (Eq. 1); the mass matrix, $[T]$, was derived from the values of the tip mass; and the coordinate transformation matrix, $[L]$, was derived relating the state variables between adjacent C-blocks using the boundary conditions. All these matrices are multiplied together to obtain a full transfer matrix for a serial C-block, $[U_i]_n$, relating the state vector at base of the serial C-block to that at the tip,

$$\{z_i\}_n|_\pi = [T][U_i]([L][U_i])^{n-1}\{z_i\}_0|_0 = [U_i]_n\{z_i\}_0|_0. \tag{5}$$

The tip and base boundary conditions are substituted into the transfer matrix equation (Eq. 5), and the resulting equation is solved to determine the natural frequencies and mode shapes of the C-block series.

To determine the full frequency-amplitude model for the C-block array, a modal analysis technique was used. The model was simplified by solving specifically for the actuation at the tip of the last C-block ($k = n$; $\theta = \pi$), yielding the magnitude of the resulting radial frequency-amplitude as

$$w_n = \frac{M^P R_n^2}{D}\sqrt{\left[2n - \sum_{i=1}^{\infty}\frac{\Lambda^2 W_i\left(\lambda_i^2 - \Lambda^2\right)}{\left(\lambda_i^2 - \Lambda^2\right)^2 + \left(\gamma\lambda_i^2\right)}\right]^2 + \left[\sum_{i=1}^{\infty}\frac{\Lambda^2 W_i\left(\gamma\lambda_i^2\right)}{\left(\lambda_i^2 - \Lambda^2\right)^2 + \left(\gamma\lambda_i^2\right)}\right]^2}. \tag{6}$$

2.1.4 Equivalent Bender Model

For large numbers of C-blocks in series, an equivalent bender model was developed, where the equivalent straight bender has the same length ($L_{eq} = 2nR_n$), mass ($\rho_{eq} = (\pi/2)\rho$), and static stiffnesses ($A_{eq} = (4D)/(pR_n^2)$, $D_{eq} = (2D/\pi)$) as the C-block array. The equivalent bender model was solved for both bending (beam) motion and extensional (rod) motion, using standard solution techniques for a straight beam (Thomson, 1988), resulting in two models: a) bending motion,

$$u_n = \frac{M^P R_n^2}{D}\left[\pi n + \sum_{i=1}^{\infty} \frac{\Lambda U_{ieq}}{\left(\lambda_{beq}^2 - \Lambda^2\right)}\right] \tag{7}$$

and b) extensional motion,

$$w_n = \frac{M^P R_n^2}{D}\left[2n + \sum_{i=1}^{\infty} \frac{\Lambda W_{ieq}}{\left(\lambda_{eeq}^2 - \Lambda^2\right)}\right] \tag{8}$$

This model accurately predicts the behavior of C-block arrays with larger numbers of C-blocks in series. For example, a series of eight C-blocks can be modeled using an equivalent straight bender approximation, with an error in natural frequency location of less than 5% for modes two and three, and less than 1% for the first mode. However, for small numbers of C-blocks in series, or for higher modes, the equivalent bender model fairs less well. For example, the equivalent straight bender overpredicts the second natural frequency of a series of two by over 30%, and overpredicts the sixth natural frequency by nearly a factor of three. Nonetheless, it is interesting to note that as the actuator array incorporates more C-blocks in series and becomes increasingly difficult to analyze, the simple equivalent bender model does a better job of predicting the behavior of the array.

2.2 Design of Experiments

A 2^k factorial experiment (Hicks 1973), which examines the nondimensional deflection (i.e. strain) of the C-block array as a function of other nondimensional parameters, was utilized to validate the accuracy of the C-block array models, determine the effect of the array design

parameters on the performance of the C-block, and demonstrate that C-block arrays can be fabricated. While other experiments have been performed on individual C-block actuators, both statically (Moskalik and Brei, 1997b) and dynamically (Moskalik and Brei, 1997a), and on serial C-blocks, also both statically (Moskalik and Brei, 1999a) and dynamically (Moskalik and Brei, 1999b), all of these were limited to specific configurations and therefore cannot be easily extended to a wider range of applications such as helicopter trailing edge flaps, micro-positioning, and complex shape control. In a 2^k factorial experimental design, the factors impacting the output parameter (strain, in this case) are determined, and a set of experiments is designed where combinations of high and low values of each factor are tested. The relative values of the output parameter resulting from this design of experiments are used to determine the effect of each factor and combination of factors on the output parameter. This provides for a wider coverage of the design space and rigorous methods to extend the results beyond the specific configurations tested.

2.2.1 Normalized Models

To reduce the number of factors impacting the output strain and simplify experimentation, the deflection term in both the static model (Eq. 3) and the dynamic model (Eq. 6) were rearranged to the left-hand side, and nondimensionalized by dividing by the length, $2nR_n$, to give

$$\frac{w_n}{2nR_n} = \frac{M^P R_n}{D} - \left(\frac{\pi}{4}\right)\frac{F_{tot}R_n^2}{mD} \tag{9}$$

for the static nondimensional model and

$$\frac{w_n}{2nR_n} = \frac{M^P R_n}{D}\sqrt{\left[1-\sum_{i=1}^{\infty}\left(\frac{W_i}{2n}\right)\frac{\Lambda^2\left(\lambda_i^2-\Lambda^2\right)}{\left(\lambda_i^2-\Lambda^2\right)^2+\left(\gamma\lambda_i^2\right)}\right]^2+\left[\sum_{i=1}^{\infty}\left(\frac{W_i}{2n}\right)\frac{\Lambda^2\left(\gamma\lambda_i^2\right)}{\left(\lambda_i^2-\Lambda^2\right)^2+\left(\gamma\lambda_i^2\right)}\right]^2} \tag{10}$$

for the dynamic model.

2.2.2 Static Design of Experiments

In the static model (Eq. 9), the strain is a function of only two nondimensional parameters: the internal moment effectiveness, M^PR_n/D, and the applied force effectiveness, $F_{tot}R_n^3/(mD)$. This leads to a 2^3 factorial design of experiments given in Table 1 with high (+) and low (-) values

of these two factors (designated "v" and "f", respectively) and the third factor of number in series ("n"). Combinations of the primary factors are shown as combinations of the designations (e.g., "v-f" for the combination of voltage and force). To complete the 2^3 matrix design, high and low values of each parameter were chosen. C-blocks were tested with two and four in series, at a high voltage of 150V and a low voltage of 15V, and with a high tip force corresponding to the blocked force and a low tip force of 0.0 N, corresponding to the free deflection.

2.2.3 Dynamic Design of Experiments

In the dynamic model, the nondimensional damping ratio, γ, is small and the orthogonality constant (W_i) and the nondimensional natural frequency (λ_i) are functions of only the number of C-blocks in series (n) and the tip mass parameter (μ). Consequently, the dynamic strain can be reduced to a function of only four parameters: internal moment effectiveness $M^P R_n/D$ (designated "v" in Table 2), forcing frequency Λ ("ω"), n ("n"), and μ ("m"). This yields the 2^4 factorial matrix design of experiments given in Table 2. To complete the 2^4 factorial matrix design, high and low values of each parameter were chosen. Actuators with two and four C-blocks in series were tested at a high voltage of 50V and a low voltage of 5V, at a high frequency between the first and second natural frequencies and a low frequency near quasi-static, and with nondimensional tip masses corresponding to 0 and 1.

2.2.4 Prototype Fabrication

For both design of experiments, only two unimorph PZT-5H prototype actuators, each similar but with a different number, n, in series (two and four) needed to be fabricated. The PZT-5H was procured in the form of 10.0 mm radius, 0.838 mm thick, 12.2 mm wide commercially available circular half-tubes with pre-plated electrodes. The material had a Young's modulus of 63 GPa and a measured piezoelectric constant of 380 pm/V. To construct the C-block substrates, strips of 0.455 mm stainless steel were cut to 12.2 mm width and bent around a double mandrel into a recursive S-shape as shown in Figure 4a. This S-shape was slightly underbent so that adjacent pieces of ceramic overlapped, which prevented the actuator from having a compliant "easier to bend" section, which alters the natural frequencies. The steel substrate was cleaned and roughened, and then bonded to the piezoceramic sections with a layer of Insulcast 501 epoxy

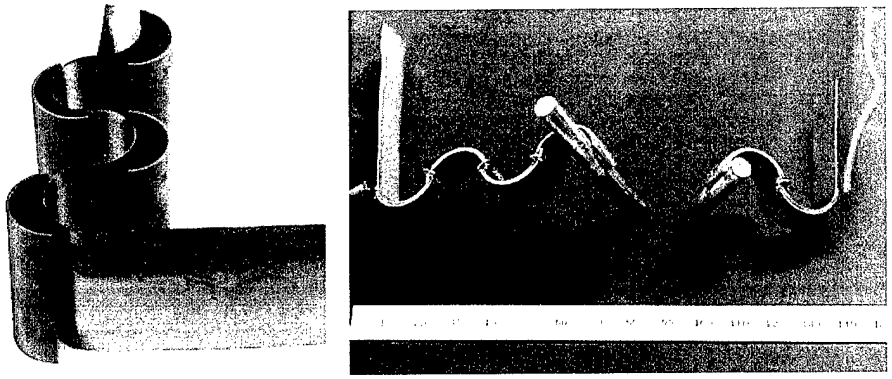

a) Ceramic and steel substrate **b) Final prototypes**

Figure 4. C-block Array Prototype Fabrication Two prototypes were fabricated to test the prototype arrays. **a)** A steel substrate was bent to conform to the inner radius of ceramic semicircles. **b)** Two prototypes were constructed, one with two in series and one with four in series. These prototypes are shown with the tip mass used for dynamic testing attached.

approximately 100 microns thick. After the epoxy cured, lead wires were soldered in between adjacent ceramics and to the base of the C-block to connect to the power supply. The completed ceramic prototypes are shown in Figure 4b.

2.2.5 Experimental Test Setup

Using the laboratory setup in Figure 5, the same two prototypes were used in three different experimental procedures: deflection-voltage, force-deflection, and frequency-amplitude. In each experiment, the C-block was clamped into place and connected to power supply: an Oregon Electronics model D4 high-voltage power supply for static tests or a Trek model 50/750 amplifier for dynamic tests. A Philtec model A88NE1 fiber optic probe was used to measure tip deflection and a Cooper instruments model LPM530 force transducer was used to measure force. The output of these transducers was monitored using a Fluke digital multimeter for the static tests or an HP model 35670A dynamic signal analyzer for the dynamic tests.

2.2.6 Deflection-Voltage Experimental Investigation

To verify the deflection-voltage model (Eq. 9 with no tip force), the radial displacement at the tip of each prototype was measured as a function of input voltage from 0V to 150V in steps of 15V. The experimental voltage and displacement values, along with the differences between

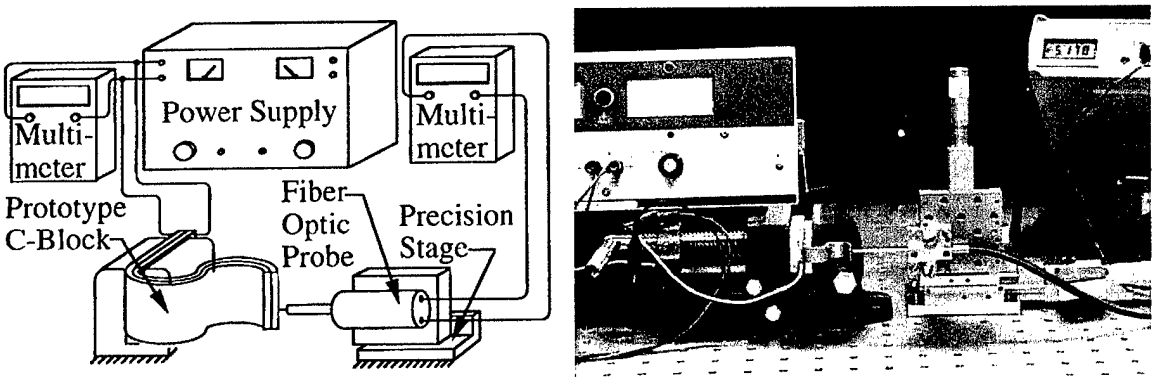

a) Diagram of test setup **b) Photograph of test setup**

Figure 5. Deflection-Voltage Experimental Apparatus for C-Block Array Prototypes The deflection of the ceramic prototypes was measured using a fiber optic probe. **a)** The diagram of the test setup shows all pieces of equipment. **b)** Photograph of test setup.

experimental results and analytical model, are given in Table 3 for both prototypes. An example graph, in this case the second prototype, is shown in Figure 6. (Additional results located in section *9.2 Additional Figures*) For both prototypes, the average difference between the experimentally observed deflection and the analytical model was 3.78% of the full-scale analytical predictions. Much of this error is due to a hysteresis effect, which was not included in the model. If the hysteresis loop is averaged out, the overall error drops to 1.75% and 1.85% for the two prototypes.

The results show a linear relation between deflection and voltage, with the commonly exhibited hysteresis. Since the nondimensional force term in Eq. (9) is eliminated, the maximum nondimensional moment effectiveness and corresponding microstrain closely agree for each prototype. Due to the slightly different construction of the two actuators, the first prototype having two C-blocks in series, had a higher nondimensional moment effectiveness at 150V than the second prototype. This resulted in a slightly higher strain (Eq. 9), and thus the first prototype exhibited slightly over half the deflection that the second prototype did. This experiment validates that the deflection output not only increases linearly with voltage, but also directly proportional to the number of C-blocks in series. This ability to tailor the deflection by combining C-blocks in series provides a major advantage to C-blocks.

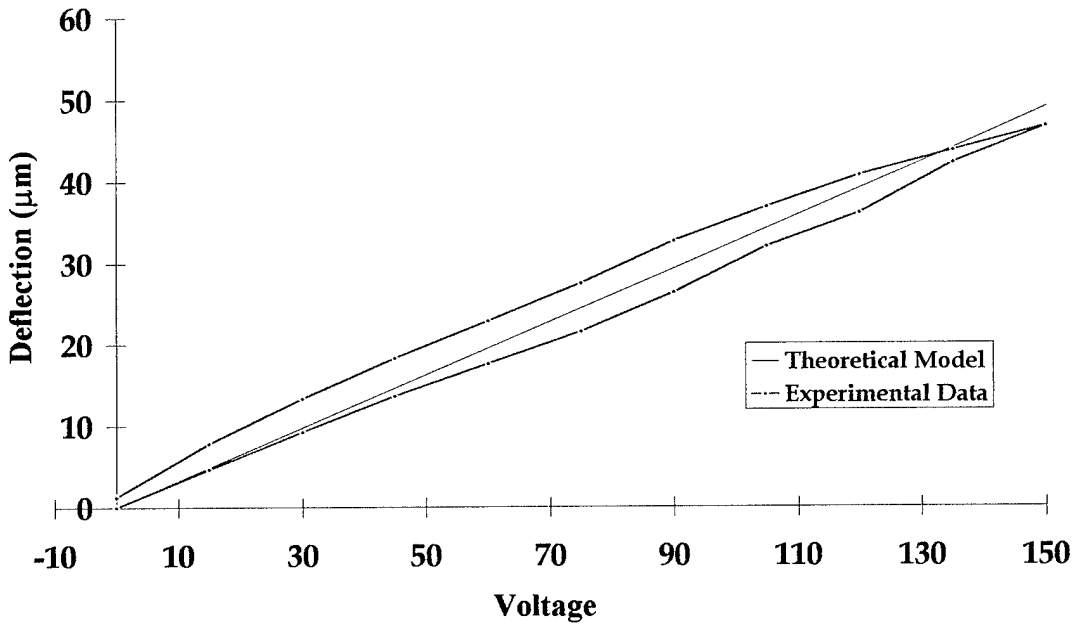

Figure 6. Deflection-Voltage Experimental Results for C-Block Array Prototype 2 These results are for a ceramic unimorph of four C-blocks with an outside radius of 10.00 mm.

2.2.7 Force-Deflection Experimental Investigation

To verify the force-deflection model (Eq. 9), the output force of each prototype was found as a function of the tip deflection while the voltage was held constant at 15V, 50V, 100V, and 150V. The maximum experimental force, as well as the averaged differences between the predicted and measured force are given in Table 4 for both prototypes at voltages of 50 V, 100 V, and 150 V. An example graph of the experimental results, in this case for the second prototype, is given in Figure 7. (Additional results located in section *9.2 Additional Figures*) The average error for all experimental runs was 3.05%, with the greatest deviation from the analytical model being 6.27%. The errors seen in the static experimentation are from nonlinear effects, such as high voltage and hysteresis effects, that are not included in the model, as well as small fabrication inaccuracies such as variations in the bonding layer thickness.

The graph of experimental results shows a linear relationship between actuator output force and deflection as input voltage is held constant, with the slope of the line indicating the stiffness of the actuator. The maximum nondimensional moment effectiveness and corresponding nondimensional force closely agree for each prototype, due to the elimination of the strain term in Eq. (7) when the deflection is zero. There is a slight, but noticeable, difference between the force

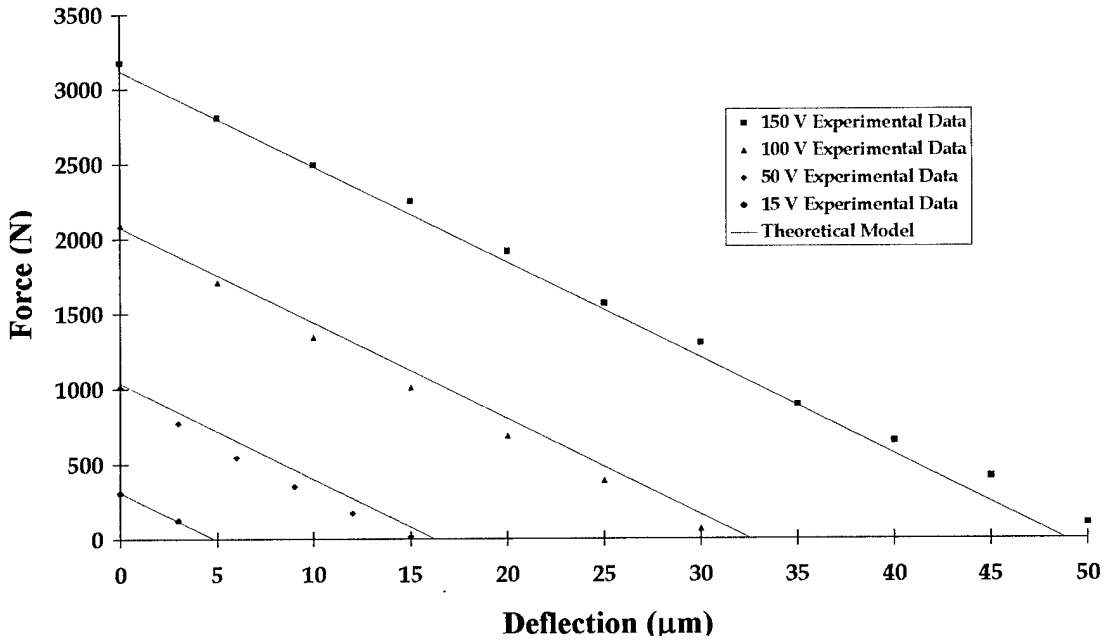

Figure 7. Force-Deflection Experimental Results for C-Block Array Prototype 2 These results are for a ceramic unimorph of four C-blocks with an outside radius of 10.00 mm.

output of the two actuators at the same input voltage, due to the increased cross-sectional stiffness, D, of the second actuator.

Data points, taken from the force-deflection experimentation were used in the 2^3 factorial analysis to calculate the effects and sum of squares for each factor (Table 1). The effects are calculated as,

$$\text{effect} = \sum(\text{strain} * \text{sign} / 4) \tag{11}$$

and indicate the relative size and sign of the effect on the output strain by that factor. The sums of squares are calculated as,

$$\text{sum of squares} = \left(\sum \text{strain}\right) - (\text{effect} * 4)^2 / 8 \tag{12}$$

and indicate the proportion of the variance in the output strain each factor accounts for.

The sums of the squares indicate that by far the greatest effects on the strain come from the nondimensional moment effectiveness (voltage), nondimensional force, and the combination of force and moment effectiveness (v-f). These three factors account for 99.7% of the total effects observed. This should be expected from examining the nondimensional static model (Eq. 9), since these are the nondimensional parameters that appear explicitly in the model. None of the factors that include the number in series produce much effect. Thus, it is apparent that the number in series has little effect on the nondimensional strain.

This analysis of the effects of each factor verifies that the linear force-deflection model (Eq. 9) is substantially correct, with no additional effects that were not included in the 2^3 factorial mode. Since the number in series, n, does not affect the strain, it is clear from Eq. (9) that the deflection (in the numerator of the strain term) is directly proportional to the number in series (in the denominator of the same term). In addition, the deflection is also linearly dependent on both the voltage and force, which indicates that both the stiffness of the actuator and actuator performance load lines are linear. The verification of the linearity of the model, and the lack of unaccounted-for effects, means that engineers can comfortably use this model to design actuators for smart structures designs.

2.2.8 Frequency-Amplitude Experimental Investigation

To verify the dynamic frequency-amplitude model (Eq. 10), the dynamic response of each prototype was found under varying loading: with and without a tip mass in place, at input voltages of 5V and 50V, and at input frequencies ranging from either 50 Hz (for series of two) or 20 Hz (for the series of four) to 10,000 Hz. The experimentally determined locations of all natural frequencies are given in Table 5 for both prototypes, and the average difference between the predicted and measured deflections and natural frequencies is given in Table 6. Additionally, an example graph is shown in Figure 8, in this case the second prototype at 50V with no tip mass. (Additional results located in section *9.2 Additional Figures*)

The average difference between the predicted and measured frequencies was 4.32% for the first prototype and 7.96% for the second prototype. The difference between the analytical and experimental values of these frequencies ranges from less than 1% to just over 14%; however, the locations of the first natural frequency are predicted much more accurately, in general, than those for higher modes. The difference in deflection averaged 3.19% of the maximum experimental amplitudes. A substantial portion of this difference is due to the slight inaccuracies in natural frequency location. The experimental results have noticeable peaks at the natural frequencies, indicating a strongly underdamped system. These nondimensional natural frequency locations are a function of the number in series, n, and the tip mass attached to the C-block, μ.

Table 2 shows that by far the greatest effect on the strain comes from the nondimensional moment effectiveness (voltage). This factor accounts for 94.9% of the total effects observed. The importance of the nondimensional moment might be expected from examining the

nondimensional dynamic model (Eq. 10) because the nondimensional moment effectiveness is directly proportional to the strain, whereas the dependence of the strain on other factors is more complex. The next three largest effects correspond to the frequency factor, series-frequency factor, and series-voltage-frequency factor, accounting for another 3.2% of the total effects. This shows that the frequency also affects the output strain; however, the amount of influence is smaller than might be expected from an examination of the dynamic model or an examination of the experimental results. This outcome is a result of the relatively simple 2^k factorial analysis not being capable of capturing the complex dependences in highly nonlinear dynamic relations; the 2^k factorial analysis is more applicable to relations that are linear, such as the static deflection-voltage or force-deflection relation.

Although the 2^4 factorial analysis does not completely reflect the accuracy of the model, the experimental results (Figure 8) demonstrate that the dynamic performance model is accurate. In addition, the series of four C-blocks showed both a reduced amplitude and frequency for the first mode in comparison to the series of two. This demonstrates that the bandwidth of longer actuators can potentially be greater than just the first mode, as the amplitude of the first mode excitation is only moderately larger than the static amplitude.

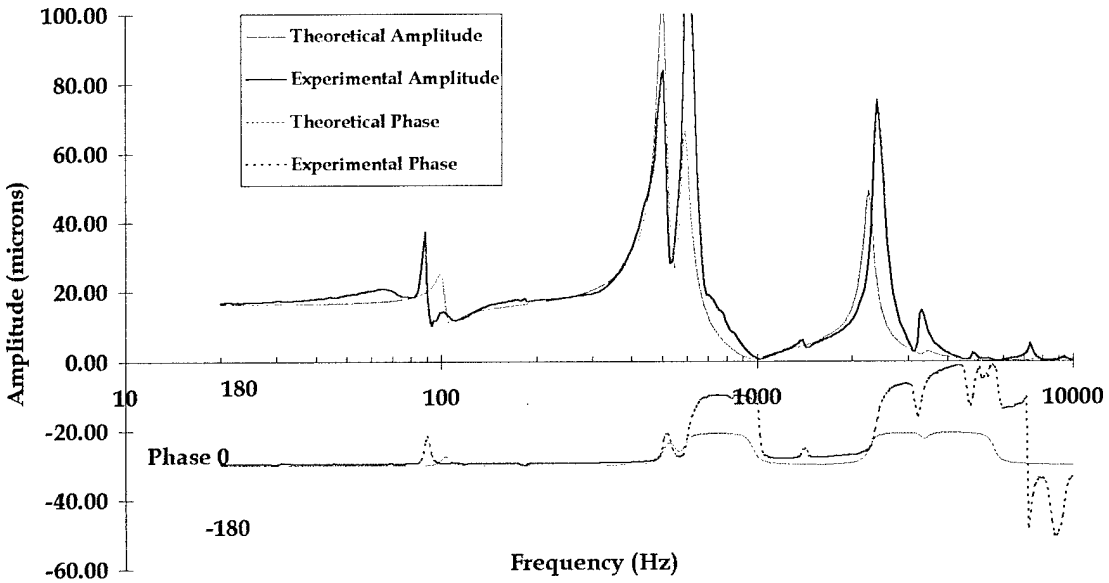

Figure 8. Frequency-Amplitude Experimental Results for C-Block Array Prototype 2 These results are for a ceramic unimorph of four C-blocks with an outside radius of 10.00 mm at 50V input with no tip mass.

3.0 ACTIVE FLAP SYSTEM DEMONSTRATION

The tailorable performance capabilities of the C-block actuators and the effectiveness of the predictive analytical models were demonstrated through the design and testing of an active flap system for applications such as rotorcraft vibration control, munitions guidance and UAV control. There has been much research with piezoelectrically driven active flaps; however, most of the current systems have flap deflections that are coupled to changes in angle of attack and airspeed. Because of this, the performance of current active flap systems is significantly degraded in the turbulent and gusting airflow associated with flight. This problem is especially evident in systems designed for active suppression of rotor blade vibrations due to the added complexities of the helicopter's domain. As the rotor sweeps the azimuth, the angle of attack of the individual blade section changes. The induced aerodynamic hinge moment can reduce the flap deflections below the 10° pp (at N/rev) which are necessary to generate the required net change in lift for vibration control. There are two main reasons for the loss in flap deflection with changes in angle of attack and increasing airspeed. The first is due to the limited actuator authority and the second is due to the flap design.

To tackle the actuation needs of the active flap systems, many different piezoelectric actuation schemes have been employed. One of the original schemes incorporated straight bimorphs which can generate large deflections but have low force (Spangler and Hall, 1990). For example, straight bimorphs that give free deflections of approximately 100 μm can only produce blocking forces on the order of 4 N (Near, 1996). Recently, researchers have overcome this by tapering the bender by adjusting the thickness of the substrate or utilizing more piezoelectric layers of varying length which can increase the output work of the straight bender (Hall and Prechtl, 1996, Koratkar and Chopra, 2000, 1997). However, the deflection, which is transverse to its length, can be an issue for active rotor blade flap systems due to interference between the bender and the surface of the rotor blade. Stacks, on the other hand, easily create the necessary force, but do not automatically generate the necessary stroke - some form of amplification is required. Unfortunately, the external leveraging systems often required to achieve large deflections can rob the actuator of as much as 80% of its energy density (Paine, and Chaudhry, 1996). Thus, many of the current piezoelectric actuation schemes cannot overcome the aerodynamic hinge moments generated as the flap is deflected.

The unique curved shape of the C-block generates approximately 2.67 times the force, and 0.405 times the deflection of a comparable straight bender, resulting in an 8% increase in work output (Moskalik and Brei, 1997b). Additionally, the curved shape allows individual C-blocks to be linked together in series, linearly increasing the actuator's deflection (deflection occurs along the actuator's length) without affecting it's blocking force (Brei, 1993). This allows the performance of a C-block actuator to be tailored directly to the application without resorting to an external leveraging system, resulting in efficient energy transfer. Additionally, the deflection of the serial C-block actuator occurs along its length, reducing the risk of interference with the surface of the wing.

Increasing the actuator authority alone does not completely overcome the airspeed and angle of attack sensitivity problem since it does not decouple the flap deflection from either of these. Most of the current active flap systems use conventional flaps with hinges near the leading edge. These flaps experience large adverse aerodynamic hinge moments as the flap is deflected; thus as airspeed is increased, the aerodynamic hinge moment increases and consequently flap deflection is significantly degraded. Similarly, the flaps have the potential of control surface lock if the aerodynamic hinge moments exceed the capabilities of the actuation system.

The C-block based active flaps are both aerodynamically and mass balanced, and thus reduce, if not eliminate, many of these problems which have plagued earlier active flaps. The mass balancing increases the frequency response by reducing the inertial load of the flap while helping to decouple the flap deflection from blade plunge motions aiding in the resistance of the flap system to control surface lock. The aerodynamic balancing nearly eliminates any moment generated by aerodynamic loads on the flap, resulting with flap deflections that are insensitive to changes in attached airflow over the blade. This characteristic of the aerodynamically balanced flap is in strong contrast to a conventional flap, where the aerodynamic loads at high speed can surpass the actuators maximum force output, thereby preventing flap deflection.

This section describes the design and wind tunnel testing of an active flap system that demonstrates the performance of the C-block actuators within the constraints of a typical design problem. For demonstration purposes, a flap system designed for rotor blade vibration suppression has been explored but the results are applicable for other active flap applications such as munitions guidance, and UAV flight control. Actuator prototypes, fabricated and tested at University of Michigan, were integrated into a dynamic rotor blade section at Auburn University

by Dr. Barrett. These actuators are approximately the size of flight-worthy hardware for an actual rotorcraft and, as a result, their large size is not directly amenable to integration in low cost University test rotors; however, they can be wind tunnel tested. Accordingly, the designed airfoil was constructed from a typical NACA 0012 rotor blade section and measures 12" in chord. It is recognized that to fully develop a rotor blade vibration reduction system, testing under the whirled condition of the helicopter flight domain are required; however, whirlstand testing was beyond the scope of this research.

3.1 Active Flap System Design

The active rotor blade flap system utilized in this research was designed from both actuation and aerodynamic standpoints simultaneously (Figure 9). Large flap deflections were achieved by designing a flap which minimize the control loads required by the actuator, and tailoring the actuator performance to the requirements of active vibration control. The trailing edge flap was mass and aerodynamically balanced flap by co-locating the center of gravity, center of pressure and flap hinge axis. As the flap is deflected, the center of pressure will shift slightly, but over a limited angular deflection range of the flap (< 15° pp), the center of pressure remains approximately on the hinge axis.

Even with the added benefits of a balanced flap, a high authority actuation system is still necessary. By concurrently designing the actuator and wing, it was determined that an actuation

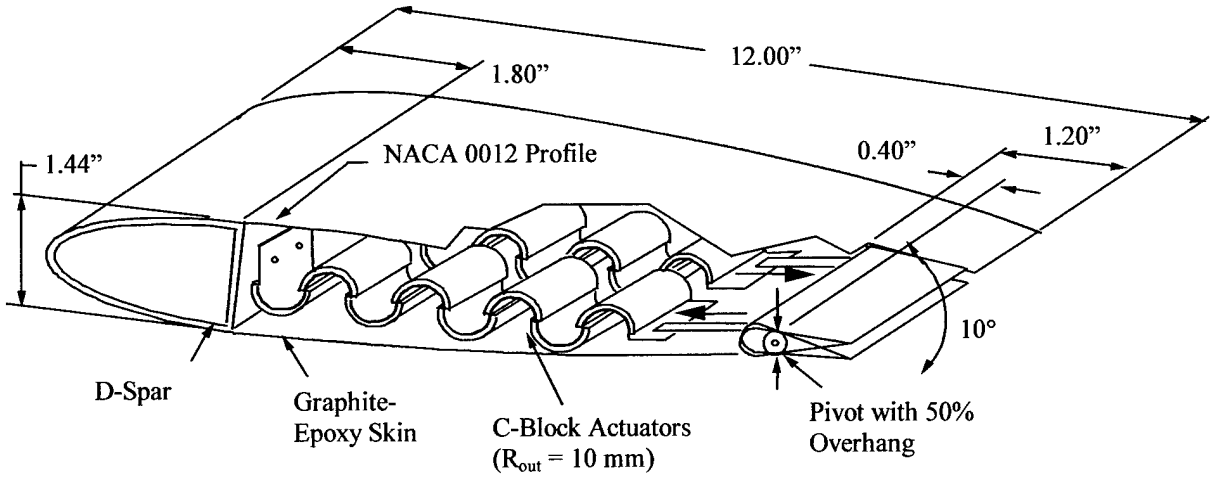

Figure 9. Active Rotor Blade System Design The wind tunnel test specimen consisted of a NACA 0012 airfoil with a 10% chord flap. The hinge axis of the flap is aligned with the center of gravity and center of pressure to reduce the inertial load and decouple the flap deflection from airspeed. The actuators are excited out of phase to drive the mass and aerodynamically balanced 10% chord flap.

system capable of a free deflection of 110 μm and a blocking force of approximately 10 N would be sufficient to generate the goal of 10° pp of flap deflection. The performance tailorability of the C-block architecture resulted in many options to meet these design requirements. A conservative actuation system was chosen which consisted of two actuators each comprised of eight C-blocks in series which should meet the required deflection and force at 2/3 the rated field (267 V/mm) of PZT-5H. Each unimorph actuator was constructed of eight PZT-5H half circles of 10mm diameter bonded to a single stainless steel substrate formed into a corrugated shape. The unimorph design was chosen for this research because it can be pre-compressed to eliminate any tensile loading in the piezoceramic material which may quickly fail the brittle ceramic actuators. These actuators were fabricated in the same way as the experimental actuators described in the section *2.0 Piezoceramic C-block Actuator Development.*

3.2 C-Block Prototype Characterization

Prior to integration with the wing section, the performance of each C-block actuator was experimentally characterized (using methods previously described in section *2.0 Piezoceramic C-block Actuator Development*) with two types of tests: the quasi-static to determine the output of the actuators in the absence of dynamic amplification, and the dynamic to verify the location of the natural frequencies and the bandwidth of the actuators. Quasi-static excitation of both actuators at 150 V (179 V/mm) resulted with free deflections of approximately 100 μm and corresponding blocking forces of approximately 10 N (Figure 10), with an average error of 5% from the analytical model. The actuators were tested dynamically over a 5000 Hz frequency range to insure that the actuators could provide vibration control at frequencies of at least 4/rev (28 Hz), a typical frequency associated with rotor blade vibrations. The first and second natural frequencies were observed at approximately 16 Hz and 250 Hz respectively (Figure 11). Both actuators displayed similar performance characteristics, which demonstrates the robustness of the actuation technology, especially in light of the imperfections introduced by hand fabrication.

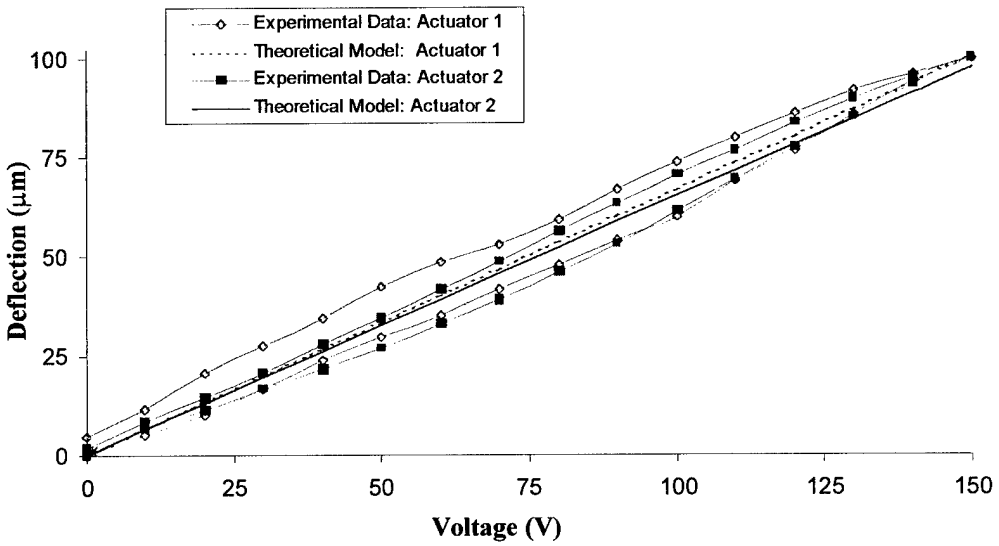

a) Deflection-Voltage Response

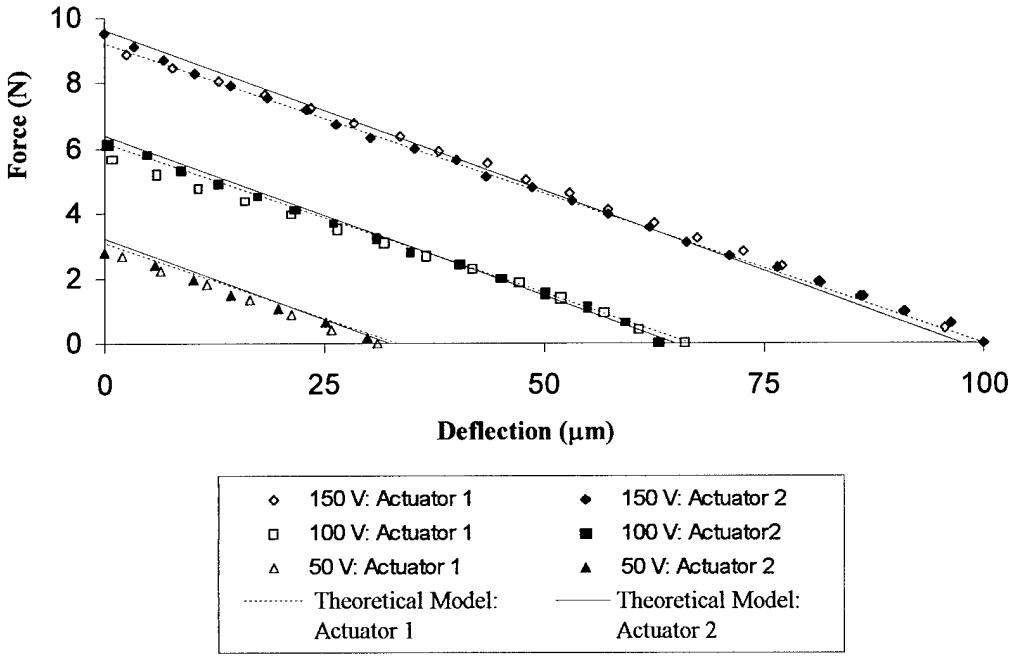

b) Force-Deflection Response

Figure 10. C-block Actuator Performance a) Deflection-Voltage Response The deflection of both actuators 1 and 2 as a function of voltage. A maximum deflection of approximately 100 μm was obtained for each actuator at 150 V (45% of the maximum rated voltage). **b) Force-Deflection Response** The force and deflection output of actuators 1 and 2 in response to input voltages of 50, 100, and 150 V. A blocking force of approximately 9.8 N was obtained for each actuator at 150 V (45% of the maximum rated voltage).

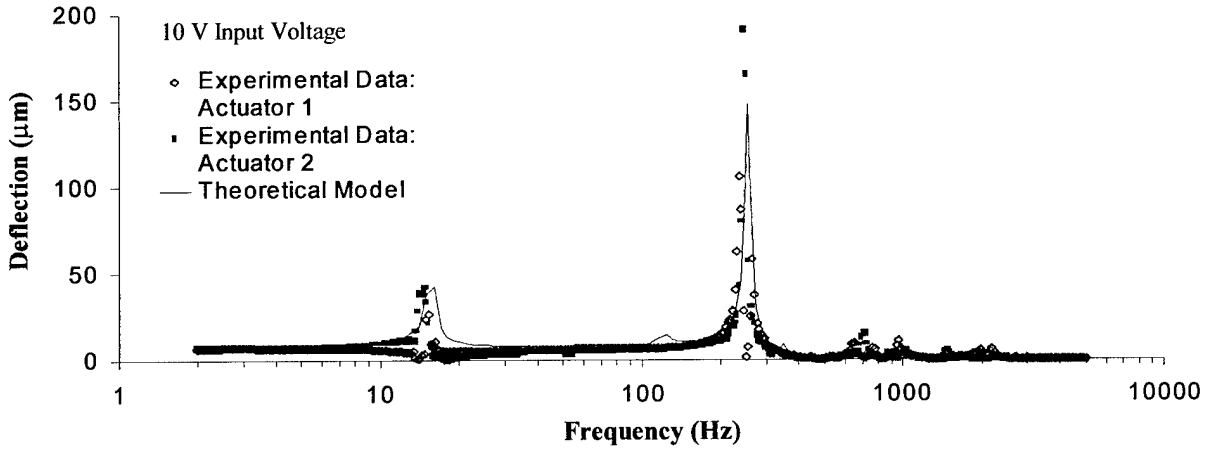

Figure 11. C-block Actuator Dynamic Response The deflection of actuators 1 and 2 in response to a sinusoidal 10 V input signal applied swept from 1 to 5000 Hz. The first and second natural frequencies were located at 16 Hz and 250Hz respectively for both actuators.

These bench-top tests confirmed that the C-block actuators could provide the necessary deflection of 110 μm to generate the desired 10° peak-to-peak of flap deflection with a bandwidth of at least 28 Hz at 44% of the maximum recommended voltage. If the voltages are increased to the maximum rated value of 335 V (~400V/mm), the actuators are expected to deflect 223 μm. This would result in a flap deflection of approximately 20° pp if no losses were incurred in the integration of the flap to the actuators. As demonstrated later, the 28 Hz bandwidth is achieved upon integration because the natural frequencies increase upon application of the pre-load applied to the actuators when bolted in the flap system. Additionally, the modal amplitude of the first natural frequency decreases because the boundary conditions are altered from the near cantilevered state during the bench-top testing of the individual actuators, to the near pinned end conditions of the actuators when connected to the flap spindle and main spar.

3.3 Active Flap System Fabrication

The 12-inch chord NACA 0012 wing section and 10% chord flap were constructed of Thornel™ graphite-epoxy cloth laid over high temperature polyester casting resin mandrels. Leading edge counter balances were added to the wing section after the C-block actuators were integrated to position the center of gravity of the entire system over the quarter-chord. The fully symmetrical NACA 0012 airfoil has an aerodynamic center located on the quarter-chord as all full symmetrical airfoils do for attached subsonic flow; thereby aerodynamically balancing attached

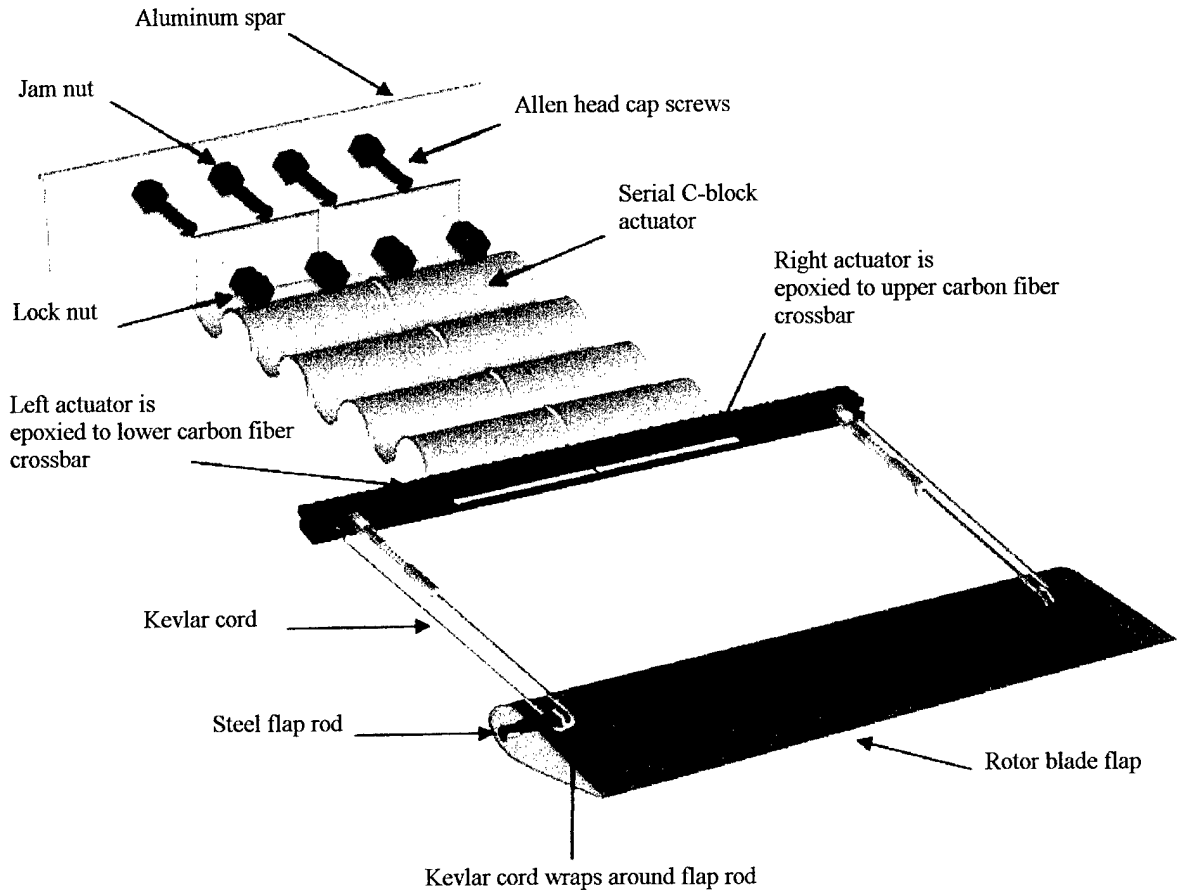

Figure 12. Integration Scheme for the Active Rotor Blade Flap System The C-blocks designed for the active rotor blade flap consisted of two side-by-side serial actuators connected to the flap spar by a Kevlar cord. The actuators are mounted to the main spar on allen head cap screws. The position of the mounting lock nuts adjusts the pre-load on the actuators to insure only compressive loads are experienced by the piezoceramic.

flow aerodynamic moments about the quarter-chord. The trailing edge flap was mass and aerodynamically balanced at the 1/3 chord position by collocating the flaps center of mass, center of pressure and hinge location.

Integration of the actuators and the blade section was critical since any unnecessary weight or friction can significantly reduce the bandwidth and the magnitude of flap deflections; therefore during integration, a concerted effort was made to minimize the inertial and frictional loading on the actuators (Figure 12). Light weight, carbon fiber crossbars were epoxied to the end of each actuator to provide an anchoring point for the Kevlar cords used to transfer the actuator deflection to the flap. The Kevlar cords were wrapped around the flap spindle and attached at either end to the crossbars. The actuators were slid onto cap screws mounted on the wing section's main spar with lock nuts while turnbuckles were used to fine-tune the tension on each

actuator during final assembly. By pretensioning the C-block actuators, the piezoceramic elements of the actuators are placed into compression, thereby diminishing the risk of ceramic fracture. The actuators were electrically isolated from the wing section and wired out of phase to drive the trailing edge flap.

3.4 Wind Tunnel Experimental Studies

Following the integration of the actuators into the flap system, a series of wind tunnel tests were conducted to verify the authority of the C-block actuators by demonstrating their ability to produce large flap deflections independent of airspeed and that these flap deflections can induce pitch changes in the entire wing section. Two types of testes were performed: fixed-wing tests, where the quasi-static and dynamic performance of the flap were examined with the wing fixed at 0° angle of attack, and free-wing tests, where the wing section was free to rotate about the ¼ chord as a result of the flap deflections. The tests were conducted in the three-foot by four-foot subsonic wind tunnel at Auburn University at airspeeds of 0, 50, and 100 and the tunnel limit of 130 ft/s. A sinusoidal input signal was supplied by a Tektronix CFG280 signal generator and amplified by a Trek 50/750 amplifier. The wing was mounted at the quarter-chord on precision bearings located on a pair of 30" square splitter plates (Figure 13). The right splitter plate was made from 0.080" thick aluminum while left splitter plate was made of ¼ inch Lexan so that the

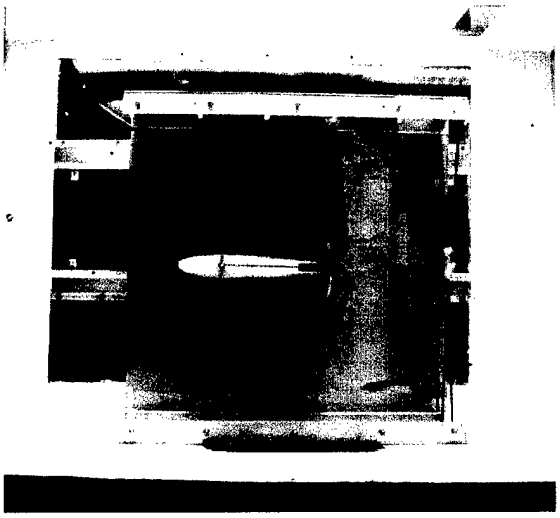

Figure 13. Wind Tunnel Test Apparatus Wind tunnel testing was conducted in the three foot by four foot subsonic wind tunnel at Auburn University. The 12" chord, 6" span, blade section was mounted between 30" splitter plates. The near plate was constructed of Lexan to allow for observation of the system.

pitch rotations could be observed. A circumferential slot was cut out of both splitter plates to allow clearance for the extension of the flap spindle beyond the span of the wing section. Electrical leads entered the wing through a small hole located just in front of the quarter-chord. The adverse pitching moments generated by the presence of the electrical leads were measured to be less than 0.01 in-oz, which was essentially negligible. Flap deflections were obtained by reflecting a laser, mounted beneath the wind tunnel, off a small mirror positioned on the flap spindle outside of the splitter plates. The reflected beam was directed onto a calibrated scale mounted inside the wind tunnel. A second calibrated scale was located on the splitter plates, along the circumferential slot, to measure the changes in the blade pitch.

3.5 Fixed Wing Flap Tests

The quasi-static flap tests were performed to determine the true performance of the system in the absence of dynamic amplification and verify that the aerodynamic balancing of the flap produced deflections that were independent of airspeed. The wing was fixed at 0° angle of attack and a 0 - 400 V (1Hz) input signal was applied to the C-block actuators while subjected to airspeeds of 0, 50, 100, and 130ft/s. The quasi-static tests demonstrated that the flap deflections in excess of 20° peak-to-peak could be commanded with minimal sensitivity to airspeed below 15° pp (Figure 14). Flap deflections above approximately 15° pp resulted in a shifting of the flap's center of pressure off the hinge axis causing the 3° pp degradation in flap deflection at 400

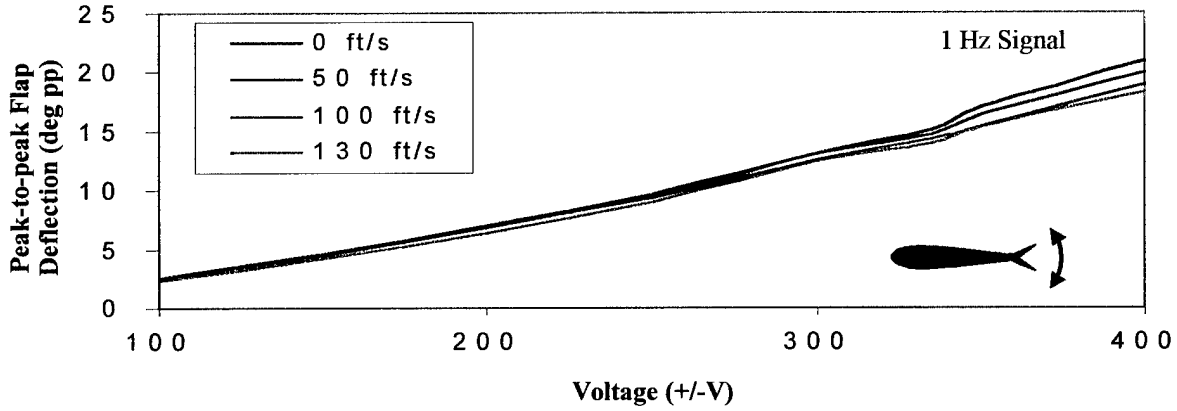

Figure 14. Quasi-static Wind Tunnel Flap Deflection Peak-to-peak flap deflection as a function of applied voltage applied at 1 Hz. Tests were conducted at airspeeds of 0, 50, and 100 ft/s with the blade section fixed at 0° pitch. The 10% chord flap reached a maximum deflection of 20.9° pp at 400 V with minimal sensitivity to airspeed below 15° pp.

V (18° pp at 130 ft/s, 21° pp at 0 ft/s). Thus, these quasi-static tests demonstrated that C-blocks could successfully drive aerodynamically balanced flaps to appreciable deflections (above 15° pp) with little degradation due to airspeed. Unlike previous approaches to adaptive flaps, which show significant loss in deflection as airspeed is increased, this system will maintain consistent levels of flap deflection independent of airspeed without requiring an oversized actuation system to overcome the large aerodynamic hinge moment inherent with conventional flaps.

A second series of fixed wing tests were conducted to explore the dynamic performance of the flap system (Figure 15) for frequencies from 0 to 80 Hz. The dynamic flap tests were performed at 0, 50, 100, and 130 ft/s with applied voltages of 100, 200, and 335 V (400 V/mm). The 200 and 335V tests were stopped at 40 Hz to reduce the risk of resonance induced damage to the system. A maximum flap deflection of 17° pp was obtained at 335 V for the maximum wind tunnel speed of 130 ft/s. Large dynamic flap deflections and a low sensitivity to airspeed were achieved for flap deflections up to 15° pp (at 335 V). Near the 58 Hz resonance, the flap deflection was reduced due to the expected increase in the aerodynamic damping associated with higher airspeeds. This degradation in flap deflection is unavoidable, but only occurs near resonance. As the system is not intended to be operated near resonance, this degradation does not impose any limitations on the active flap system.

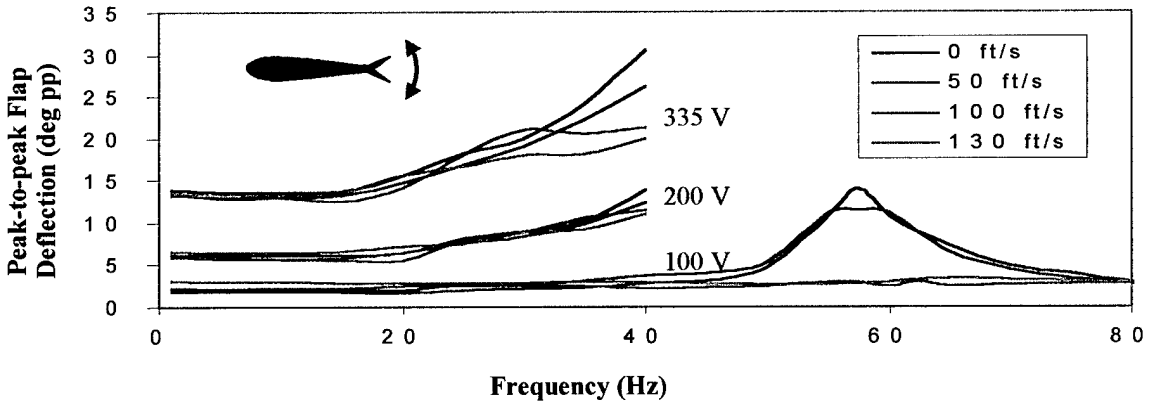

Figure 15: Dynamic Wind Tunnel Flap Response The dynamic response of the flap with the blade section fixed at 0° pitch was examined over a 100 Hz frequency range. The first significant resonance peak was observed at 58 Hz. Flap deflections were observed to be highly insensitive to airspeed for deflections under 15° pp for all airspeeds tested. At 28 Hz, the frequency associated with the predominant vibration loads on a helicopter, flap deflections in excess of 17° pp were obtained at 400 V/mm for all airspeeds tested.

The fixed wing tests proved that aerodynamic and mass balancing the flap, combined with the high authority C-block actuators, results in large flap deflections that are insensitive to airspeed. As a result, the active flap system should not experience significant performance degradation in response to the gust loads prevalent in helicopter flight. The flap could be commanded over a 58 Hz frequency range, representing the potential to control many modes of vibration. The 58 Hz bandwidth of the 12" chord test specimen corresponds to approximately 8.5/rev, considering a 46% scale YUH-61 rotor system, or 8.8/rev, considering a 92% scale OH-58 rotor system, or 9.8/rev, considering a 178% scale Boeing 500E rotor blade. Thus, the system has the potential of handling most HHC or IBC system commands, even for the five-bladed 500E rotor system.

3.6 Wing Pitch Deflection Experiments

Following the fixed wing testing, the wing was unlocked and allowed to rotate freely about the quarter-chord to demonstrate the ability of the flap to induce a pitching moment on the entire wing. This study was based on a 6 in span wing section and not a full wing or rotor blade, as such, the results are only intended to demonstrate that the C-block driven balanced flap can indeed create significant hinge moments about the wing's quarter-chord. Further testing of a more complete wing was out of the scope of this research but will be necessary to fully validate the active flap system for flight control applications. The wing section was mass and aerodynamically balanced about the quarter-chord so that only unsteady aerodynamic and inertial loads were present. Two series of tests were conducted to measure the wing pitch deflections in response to both static and dynamic flap deflections. The response of the wing to near static

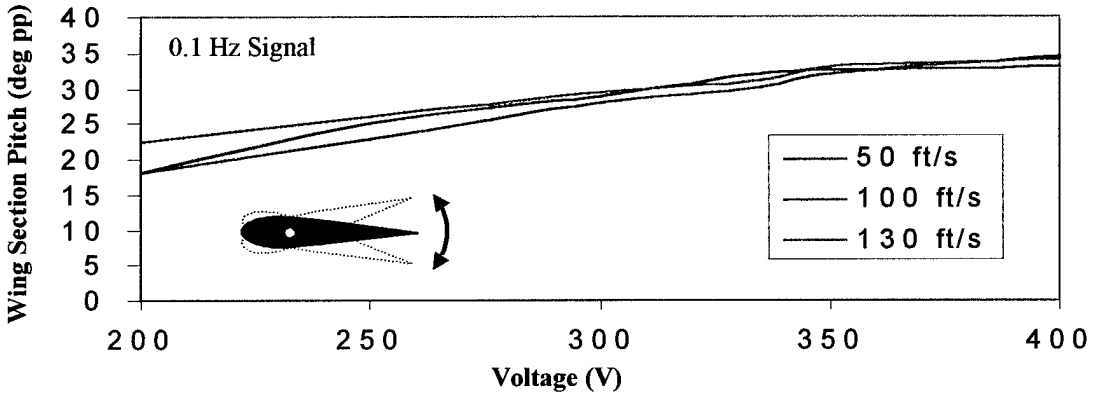

Figure 16. Static Blade Pitch Response The blade section was allowed to pivot around the quarter-chord in response to flap deflections. Low frequency (0.1 Hz) testing at airspeeds from 0 to 130 ft/s resulted in a maximum blade pitch of 33° pp with minimal sensitivity to airspeed.

(~0.1 Hz) flap deflections was examined to determine the system's performance isolated from any unsteady aerodynamic and inertial moments. The test was performed by applying a 200-400 V sinusoidal input to the C-block actuators and measuring the wing's pitch as a result of the flap's deflection for tunnel speeds of 50, 100, and 130 ft/s. Wing pitch increased smoothly for all airspeeds tested reaching the maximum measured pitch of 33° pp at 400 V (Figure 16). Because most rotor blade systems operate with blade pitch deflections on this order, the C-block driven active flap system shows potential for full flight control as well as HHC and IBC.

The dynamic response of the wing section was examined to verify the system's potential for applications such as UAV guidance and main collective control of rotorcraft at airspeeds of 50, 100 and 130 ft/s (Figure 17). For each voltage, the actuator excitation frequency was increased from 0.1 Hz to 10 Hz. Pitch deflection and bandwidth were observed to increase with airspeed due to the rise in the aerodynamic control moment associated with the increased airflow. Maximum pitch deflections of 40° pp (test setup limited) were obtained at the natural frequency of 3 Hz. It is easy to see that wind tunnel testing at speeds of 600 ft/s would yield a significantly higher system bandwidth. Indeed, at full power and 600 ft/s, the aerodynamic control moments increase to 21 times the level tested, leading to a blade corner frequency of 13.8 Hz. This corresponds to 2.1/rev full blade pitch deflections on a full-scale Bell 206 (which has a 13 in. chord). Given that the C-Block rotor blade section was optimized neither for mass nor inertia minimization, still further improvements to bandwidth levels beyond 3/rev are possible. Accordingly, this system is well suited for control of HHC and IBC commands as well as flight control from static through N+1/rev actuation frequencies.

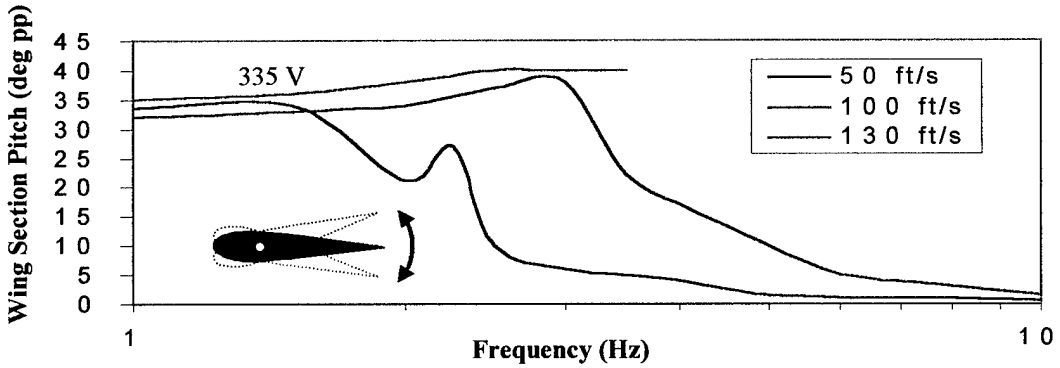

Figure 17. Dynamic Blade Pitch Response The dynamic blade pitch deflection in response to a 1 - 10 Hz flap deflection was examined at tunnel speeds of 50, 100, and 130 ft/s. Resonance occurred at approximately 3 Hz for the high voltage run (335 V) resulting in a test setup limited deflection of 40° pp. The 3 Hz bandwidth demonstrates the potential to augment collective blade control.

4.0 CONCLUSIONS

Crucial to the success of any active flap system is the design of its actuators. In this research, an innovative actuator technology was developed and validated by achieving promising experimental results, demonstrating that the technology is suitable for active flap control. This research developed and experimentally validated, using a 2^k factorial design of experiments, simple predictive analytical models which can capture the complex response of the generalized C-block actuator to within 15 % (in most cases substantially lower). The static models show that the deflection of the C-block array increases linearly with the number in series, and the force increases linearly with the number in parallel. In addition, both force and deflection performances are linear functions of the input voltage. The dynamic models show that the C-block array has identifiable natural frequencies, which can be accurately predicted. For larger arrays containing more C-blocks in series, the behavior of the C-block array reduces to that of an equivalent straight bender, and thus a simpler straight bender model can be used to design large arrays. Thus analytical models describing the behavior of the C-block array are simple in form and can be used by engineers to design C-block arrays for a number of applications such as munitions guidance, UAV control and rotorcraft vibration suppression.

For an active flap system to prove viable for applications such as rotor blade vibration suppression, it must be capable of large flap deflections which are insensitive to airspeed. This property has been successfully demonstrated utilizing C-block actuators coupled to an aerodynamically and mass balanced trailing edge flap. Large flap deflections in excess of 15° pp were obtained with no significant sensitivity to airspeed while providing a sufficient bandwidth (58 Hz) for most HHC and IBC commands. By providing flap deflections of sufficient magnitude for vibration suppression and decoupling theses deflections form airspeed, the potential for active blade control in the gusting environment of the helicopter has been demonstrated. Additionally, a potential for main collective control as well as full flight control of subsonic craft such as UAV, was demonstrated by dynamic wing pitch deflections in excess of 40° pp and a 3 Hz bandwidth.

Current research has demonstrated that the derived analytical models can successfully capture the response of a generalized C-block actuator and be used to design actuation systems for real world applications. As this research was meant to simply demonstrate the feasibility of the C-block actuator, some testing necessary to fully validate the active flap system was omitted. A

determination of the failure modes is necessary before the C-clock actuators could be safely installed into a real world application. Because the failure modes are highly dependent on the specific application, an actuation system specifically designed for a given application must be first designed and then tested. Additional wind tunnel testing across the intended flight speeds is necessary to demonstrate the insensitivity of the active flap design to all airspeeds in the desired flight envelope. For the rotor blade vibration suppression application, whirlstand testing is necessary to capture the added centrifugal loading on both the actuator and flap. Developing a system for whirlstand testing will require a modified actuation system, active flap, and system integration method to withstand the added centrifugal loading.

Despite the limited scope of this research, this research has demonstrated that C-blocks can successfully meet the midrange deflection and force requirements of applications such as active flap control in a highly mass efficient actuation package. The development of the C-block actuator technology allows engineers to design distributed C-block array architectures, thus improving the performance and versatility of actuator systems over those currently available. The contributions of C-blocks lie in their ability to fill the current midrange performance gap in actuator capabilities and expand the applications where smart structures can be successfully used, both in military applications such as helicopter rotors, airfoil shaping, fine targeting of munitions, and vibration control of sensitive equipment, and in civilian applications such as fuel injectors, engine mounts, machine tool vibration control, and medical probe positioning.

5.0 PUBLICATIONS AND TECHNICAL REPORTS

Ph.D. Theses

1. Moskalik, A. J., 1999, *Design and Characterization of C-block Actuators: Individual and Array Architectures*, PhD Dissertation, University of Michigan.

Refereed Journal Papers

2. Brei, D., and Moskalik, A. J., 1997, "Deflection Performance of a Bi-Directional Polymeric Piezoelectric Microactuator," *IEEE/ASME Journal of Microelectromechanical Systems,* Vol. 6, No. 1, pp. 62-69.

3. Moskalik, A. J., and Brei, D., 1999, "Dynamic Performance of C-Block Array Architectures," conditionally accepted with minor revisions to the *Journal of Sound and Vibration.*

4. Moskalik, A. J. and Brei, D., 1999, "Force-Deflection Behavior of Piezoelectric C-Block Actuator Arrays," *Smart Materials and Structures*, Vol. 8, pp.531-543.

5. Moskalik, A. J., and Brei, D., 1998, "Analytical Dynamic Performance Modeling for Individual C-Block Actuators," *Journal of Vibrations and Acoustics*, Vol. 121, pp. 221-230.

6. Moskalik, A. J., and Brei, D., 1998, "Parametric Investigation of the Deflection Performance of Serial Piezoelectric C-Block Actuators," *Journal of Intelligent Material Systems and Structures*, Vol. 9, pp. 223-231.

7. Moskalik, A. J., and Brei, D., 1997, "Deflection-Voltage Model and Experimental Results for Polymeric Piezoelectric C-Block Actuators," *AIAA Journal,* Vol. 35, No. 9, pp.1556-1558. (Technical Note)

8. Moskalik, A. J., and Brei, D., 1997, "Quasi-Static Behavior of Individual C-Block Piezoelectric Actuators," *Journal of Intelligent Material Systems and Structures*, Vol. 8, No. 7, pp. 571-587.

Refereed Conference or Symposium Proceedings

9. Brei, D., Ervin, J., and Moskalik, A. 1996, "Deflection-Voltage Performance of Asymmetrically Activated Piezoelectric C-Block Actuators," in *Smart Structures and Materials 1996: Smart Structures and Integrated Systems,* Inderjit Chopra, Ed., Proc. SPIE 2717, pp. 276-286 (presented at the SPIE Smart Structures and Materials Conference, San Diego, CA, February 1996).

10. Clement, J. W., Brei, D., Moskalik, A. J., and Barrett, R., 1999, ""Wind Tunnel Testing of a High Authority Airspeed Insensitive Rotor Blade Flap", AIAA-99-1503, 40th AIAA/ASME/ASCE/AHS/ASC Structures, Structural Dynamics and Materials Conference and Exhibit, St. Louis, MO, April 12-15, 1999,Vol. 4, pp. 2414-2424.

11. Clement, J. W., Brei, D., Moskalik, A. J., and Barrett, R., 1998,"Bench-Top Characterization of an Active Rotor Blade Flap System Incorporating C-Block Actuators," AIAA-98-2108, 39th AIAA/ASME/ASCE/AHS/ASC Structures, Structural Dynamics and Materials Conference and Exhibit, Long Beach, CA, Apr. 20-23, 1998. Vol. 4, pp. 2857-2869.

12. Moskalik, A. J., and Brei, D., 1998, "Force-Deflection Characterization of Series Arrays of Piezoelectric C-Block Actuators," in Smart Structures and Materials 1998: Smart Structures and Integrated Systems, Proc. SPIE 3329, pp. 659-669 (presented at the SPIE Smart Structures and Materials Conference, San Diego, CA, March 1998).

13. Moskalik, A. J., and Brei, D., 1997, "Frequency-Amplitude Response of Individual Piezoelectric C-Block Actuators," in *Smart Structures and Materials 1997: Smart Structures and Integrated Systems,* Proc. SPIE 3041, M. E. Regelbrugge, Ed., pp. 482-495 (presented at the SPIE Smart Structures and Materials Conference, San Diego, CA, March 1997).

14. Moskalik, A. J., and Brei, D., 1996, "Force-Deflection Behavior of Individual Unimorph Piezoceramic C-Block Actuators," in *Proceedings of the ASME Aerospace Division, AD-Vol. 52,* J. C. I. Chang, J. Coulter, D. Brei, D. Martinez, W. Ng, and P. P. Freidmann, Eds, pp.679-687 (presented at the ASME 1996 International Mechanical Engineering Conference and Exposition, Atlanta, GA, November 1996).

Abstracts/Posters in Refereed Conference Proceedings

15. Moskalik, A. J. and Brei, D., 1998, "Dynamic Behavior of Serial C-Blocks," presented at the 13th US National Congress of Applied Mechanics, Gainesville, FL, June.

16. Moskalik, A. J., and Brei, D., Palko, S. J. and Barrett, R. 1997, "Deflection Response for Series Configurations of Piezoceramic Unimorph C-Block Actuators," presented at the 3rd ARO Workshop on Smart Structures, Blacksburg, VA, August 1997.

17. Moskalik, A. J., and Brei, D., 1996, "A Novel PZT Bender with Enhanced Force-Voltage Performance," presented at the 33rd Annual Technical Meeting of the Society of Engineering Science, Tempe AZ, October 1996.

18. Brei, D. and Barrett, R., September 1997, "Development of a Balanced Active Rotor Blade Flap Using Piezoceramic C-block Actuators", Air Force Office of Scientific Research / Army Research Office Workshop, Myrtle Beach, SC.

19. Brei, D. and Moskalik, A.J., January 1998, "Proof-of-Concept Study of Piezoceramic C-block Actuators", 1998 NSF Design and Manufacturing Grantees Conference, Monterrey, Mexico.

6.0 PARTICIPATING PERSONNEL

Dr. Diann Brei, Principal Investigator
University of Michigan
Mechanical Engineering Department
2250 G.G. Brown Building
2350 Hayward Street
Ann Arbor, MI 48109-2125
dibrei@engin.umich.edu
(734) 763-6617

Dr. Ron Barrett, Co-Principal Investigator
Auburn University
Aerospace Engineering Department
211 Aerospace Engineering Building
Auburn, Alabama 36849-5338
rbarrett@eng.auburn.edu
(205) 844-6825

Dr. Andrew Moskalik, Graduate Student
Graduated with Doctor of Philosophy in Mechanical Engineering, December 1998
Employed as: Mechanical Research Engineer, Advanced Technology Support Division
United States Environmental Protection Agency
National Vehicle & Fuel Emissions Laboratory
2565 Plymouth Road
Ann Arbor, MI 48105
moskalik.andrew@epamail.epa.gov
(734) 214-4719

Joseph Clement, Graduate Student
Graduated with Master of Science in Mechanical Engineering, December 1999
Continuing as doctoral student
University of Michigan
Mechanical Engineering Department
2250 G.G. Brown Building
2350 Hayward Street
Ann Arbor, MI 48109-2125
jwclemen@engin.umich.edu
(734) 764-9156

7.0 REPORT OF INVENTIONS

No inventions resulted from this research.

8.0 BIBLIOGRAPHY

August, J.A. and Joshi, S.P., 1996, "Preliminary Design of Smart Structure Fins for High-Speed Missiles", in *Smart Structures and Materials 1996: Industrial and Commercial Applications of Smart Structures Technologies,* C. R. Crowe, Ed., Proc. SPIE 2721, pp. 58-65.

Barrett, R., 1990a, "Intelligent Rotor Blade Actuation through Directionally Attached Piezoelectric Crystals," presented at the *AHS National Forum,* Washington, D.C..

Barrett, R., 1990b, *Intelligent Rotor Blade and Structures Development Using Directionally Attached Piezoelectric Crystals*, M.S. Thesis, University of Maryland, College Park, MD.

Barrett, R., 1990c, "Method and Apparatus for Structural Actuation and Sensing in a Desired Direction," *U. S. Patent Application 485,599/07.*

Barrett, R., 1993a, "Modeling Techniques and Design Principles of a Low Aspect Ratio Active Aeroservoelastic Wing," *Proceedings of the North American Conference on Smart Materials and Structures,* Albuquerque, New Mexico, pp. 107-118.

Barrett, R., 1993b, "Active Composite Torque-Plate Fins for Subsonic Missiles," paper presented at the Dynamic Response of Composite Structures Conference, New Orleans, Louisiana.

Barrett, R., 1993c, "Advanced Low-Cost Smart Missile Fin Technology Evaluation," Final Report to Wright Laboratory, USAF Armament Directorate, contract number F08630-93-C-0039 Eglin AFB.

Barrett, R., 1994a, "A Solid State Apparatus for Controlling Pitch Deflections of Aerodynamic Flight Control Surfaces," Auburn University invention disclosure, patent pending.

Barrett, R., 1994b, "Active Plate and Missile Wing Development Using DAP Elements," *AIAA Journal,* Vol. 32, No. 3, pp. 601-609.

Barrett, R., 1994c, "All-Moving Active Aerodynamic Surface Research," presented at the 31st Annual Technical Meeting of the Society of Engineering Science, College Station, TX.

Barrett, R., Gross, R. S., and Brozoski, F., 1995, "Missile Flight Control using Active Flexspar Actuators," paper presented at the 1995 Smart Structures and Materials Conference, San Diego, California.

Baz, A., and Poh, S., 1988, "Performance of an active control system with piezoelectric actuators," *Journal of Sound and Vibration*, Vol. 126, pp. 327-343.

Ben-Zeev, O., and Chopra, I., 1996, "Advances in the development of an intelligent rotor employing smart trailing edge flaps," *Smart Materials and Structures*, 5: pp. 11-25.

Brei, D., 1993, "The Development of a Polymeric Piezoelectric Bimorph Microactuator-Based Macroactuator for an Artificial Hand," *PhD Thesis: Arizona State University.*

Chopra, I., 1996, "Review of current status of smart structures and integrated systems," in *Smart Structures and Materials 1996: Smart Structures and Integrated Systems,* I. Chopra, Ed., Proc. SPIE 2717, SPIE, Bellingham, WA, pp. 20-62.

Damjanovic, D., and Newnham, R. E., 1992, "Electrostrictive and piezoelectric materials for actuator applications," *Journal of Intelligent Material Systems and Structures*, Vol. 3, No. 2, pp. 190-208.

Duvernier, M., Reithler, L., Guerrero, J.Y., Ross, R., 2000, "Active Control System for a Rotor Blade Trailing-Edge Flap," in *Smart Structures and Materials 2000: Smart Structures and Integrated Systems*, N. Wereley, Ed. SPIE Vol. 3985: 52-61.

Face International, 1997, "THUNDER Sensors and Actuators" [brochure], available from Face International, 427 W. 35th St., Norfolk VA 23508.

Fulton. M. V. and Ormiston R. A., 1998, "Wind Tunnel Results for Small-Scale Rotor with On-Blade Elevons," *Proc. AHS 54th Annual Forum*, Alexandria, Virginia, pp 433-451.

Fulton. M. V. and Ormiston R. A., 1997, "Hover Testing of a Small-Scale Rotor with On-Blade Elevons," *Proc. AHS 53rd Annual Forum*, Virginia Beach, Virginia, April 29-May 1.

Giurgiutiu, V., Rogers, C. A., and Rusovici R., 1996, "Solid-State Actuation of Rotor Blade Servo-flap for Active Control," *Journal of Intelligent Material Systems and Structures*, 7:192-202.

Giurgiutiu, V., 2000, "Recent Advances in Smart-Material Rotor Control Actuation," *in Proceedings of the 41st Structures, Structural Dynamics and Materials Conference*, Atlanta, Georgia, April 3-6.

Haertling, G. H., 1994, "Ultra-High-Displacement Actuator," *American Ceramic Society Bulletin*, Vol. 73, pp. 93-96.

Hall, S. R., and Prechtl, E. F., 1996, "Development of a piezoelectric servoflap for helicopter rotor control," *Smart Materials and Structures*, Vol. 5, pp. 26-34.

Hall, S.R., Tzianetopoulou, T., Straub, F., Ngo, H., 2000, "Design and testing of a double X-frame piezoelectric actuator," in *Smart Structures and Materials 2000: Smart Structures and Integrated Systems*, N. Wereley, Ed. SPIE Vol. 3985: 26-36.

Hicks, C. R., 1973, *Fundamental Concepts of Design of Experiments*, 2nd ed., Holt, Rinehart, and Winston, New York.

Hoppe, R., 1871, "Vibrationen eines ringes in seiner ebene," *Journal fur die Reine und Angewandte Mathematik (Crelle's Journal),* Vol. 73, pp. 158-170.

Koratkar, N.A. and Chopra, I., 1997, "Testing and Validation of a Froude scaled Helicopter Rotor model with Piezo-Bimorph actuated Trailing Edge Flaps," in *Smart Structures and Materials 1997: Smart Structures and Integrated Systems*, M. Regelbrugge, Ed. SPIE Vol. 3041: 183-205.

Koratkar, N.A. and Chopra, I., 2000, "Hover Testing of Mach-Scaled Rotor with Piezoelectric Bender Actuated Trailing-Edge Flaps," in *Smart Structures and Materials 2000: Smart Structures and Integrated Systems*, N. Wereley, Ed. SPIE Vol. 3985: 2-10.

Kugel, V. D., Chandran, S., and Cross, L. E., 1997, "Comparative analysis of piezoelectric bending-mode actuators," in *Smart Structures and Materials 1997: Smart Materials Technologies*, W. C. Simmons, I. A. Aksay, and D. R. Huston, Eds., Proc SPIE 3040, SPIE, Bellingham, WA, pp. 70-80.

Larson, P. H., and Vinson, J. R., 1993a, "On the analysis of adaptive shell structures employing piezoelectric materials," in *Proceedings of the American Society for Composites Eighth Technical Conference*, pp. 141-150.

Larson, P. H., and Vinson, J. R., 1993b, "The use of piezoelectric materials in curved beams and rings," *Adaptive Structures and Material Systems: AD-Vol. 35*, ASME, New Yourk, pp. 277-285.

Lee, T. and Chopra, I., 2000, "Development of a Smart Trailing-Edge Flap Actuator with Multi-Stage Stroke Amplification," in *Smart Structures and Materials 2000: Smart Structures and Integrated Systems*, N. Wereley, Ed. SPIE Vol. 3985: 11-25.

Lee, T. and Chopra, I., 1999, "Development and Validation of a Refined Piezostack-Actuated Trailing-Edge Flap Actuator for a Helicopter Rotor," *Proceedings of the SPIE Conference on Smart Structures Materials*, Newport Beach, CA, SPIE Vol. 3668: 22-36

Love, A. E. H., 1944, *A Treatise on the Mathematical Theory of Elasticity*, 4th ed., Dover, New York.

Meirovitch, L., 1967, *Analytical Methods in Vibration*, Macmillan, New York.

Moskalik, A. J., 1999, *Design and Characterization of C-block Actuators: Individual and Array Architectures*, PhD Dissertation, University of Michigan.

Moskalik, A. J. and Brei, D., 1997a, "Frequency-Amplitude Response of Individual Piezoelectric C-Block Actuators," in *Smart Structures and Materials 1997: Smart Structures and Integrated Systems*, Proc. SPIE 3041, M. E. Regelbrugge, Ed., pp. 482-495.

Moskalik, A. J., and Brei, D., 1997b, "Quasi-Static Behavior of Individual C-Block Piezoelectric Actuators," *Journal of Intelligent Material Systems and Structures*, Vol. 8, No. 7, pp. 571-587.

Moskalik, A. J. and Brei, D., 1999a, "Force-Deflection Behavior of Piezoelectric C-Block Actuator Arrays," *Smart Materials and Structures*, Vol. 8, pp.531-543.

Moskalik, A. J., and Brei, D., 1999b, "Dynamic Performance of C-Block Arrays," submitted to the *Journal of Sound and Vibration.*

Near, C. D., 1996, "Piezoelectric actuator technology," in *Smart Structures and Materials 1996: Smart Structures and Integrated Systems*, I. Chopra, Ed., Proc. SPIE 2717, SPIE, Bellingham, WA, pp. 246-258.

Qatu, M. S., 1993, "Theories and analysese of thin and moderately thick laminated composite curved beams," *International Journal of Solids and Structures*, Vol. 30, pp. 2743-2756.

Paine, J.S.N., and Chaudhry, Z., 1996, "The impact of amplification on efficiency and energy density of induced strain actuators," in *Proceedings of the ASME Aerospace Division*, New York: ASME, 511-516.

Pestel, E. and Leckie, F. A., 1963, *Matrix Methods in Elastomechanics*, McGraw-Hill, New York.

Prechtl, E. F. and Hall, S. R., 1999, "Design of a high efficiency, large stroke, electromechanical actuator," *in Smart Materials and Structures*, v 8 n 1 Feb 1999. pp 13-30

Prechtl, E. F. and Hall, S. R., 1997, "Design of a High Efficiency Discrete Servo-Flap Actuator for Helicopter Rotor Control," in *Smart Structures and Materials 1997: Smart Structures and Integrated Systems*, M. Regelbrugge, Ed. SPIE Vol. 3041: 158-182.

Rusovici, R. and Cudney, H. H., 1997, "Design and Testing of a Helicopter Trailing Edge Flap with Piezoeletric Stack Actuators," *in Smart Structures and Materials 1997: Smart Structures and Integrated Systems*, M. Regelbrugge, Ed. SPIE Vol. 3041: 146-157.

Samak, D. K. and Chopra, I., 1993, "A Feasibility Study to Build a Smart Rotor: Trailing Edge Flap Actuation," *Proceedings of the 1993 North American Conference on Smart Structures and Materials,* Albuquerque, NM, pp. 225-237.

Samak, D.K. and Chopra, I., 1994, "Design of High Force, High Displacement Actuators for Helicopter Rotors," *Proceedings of the 1994 North American Conference on Smart Materials and Structures*, Orlando, FL., pp. 86-97.

Shoup, T. E., 1971, "Shock and vibration isolation using nonlinear elastic suspension," *AIAA Journal*, Vol. 10, pp. 559-560.

Shoup, T. E., 1972, "Experimental investigation of a nonlinear elastic suspension," *AIAA Journal*, Vol. 9, pp. 1643-1645.

Shoup, T. E., and Simmonds, G. E., 1977, "An adjustable spring rate elastic suspension," *AIAA Journal*, Vol. 15, pp. 865-866.

Spangler, R. L. and Hall, S. R., 1990, "Piezoelectric Actuators for Helicopter Rotor Control," Paper No. 90-1076-CP, *Proceedings of the 31st Structures, Structural Dynamics and Materials Conference*, Long Beach, California, April 2-4.

Straub, F. K. and Merkley, D. J, 1997, "Design of a smart material actuator for rotor control," *Smart Materials and Structures*, 6:26-34.

Spencer T. and Chopra I., 1996, "Design and Testing of a Helicopter Trailing Edge Flap with Piezoeletric Stack Actuators," *in Smart Structures and Materials 1996: Smart Structures and Integrated Systems*, I. Chopra, Ed. SPIE Vol. 2717: 120-131.

Sugawara, Y., Onitsuka, K., Yoshikawa, S., Xu, Q. C., Newnham, R. E., and Uchino, K., 1992, "Metal-ceramic composite actuators," *Journal of the American Ceramic Society*, Vol. 75, pp. 996-998.

Thompson, W. T., 1988, *Theory of Vibration with Applications*, 3rd ed., Prentice-Hall, Englewood Cliffs, N. J.

9.0 APPENDIX

9.1 Nomenclature

b	layer cross-sectional width
$d31$	piezoelectric constant
k	iteration variable on number of C-blocks in series
m	number of C-blocks in series in the array
n	number of C-blocks in parallel in the array
q	number of layers in a C-block
t	time
u	circumferential motion of individual C-block; transverse motion of series
w	radial motion of individual C-block; longitudinal motion of series
z	layer distance form the neutral axis
$\{z\}$	state variable vector
A	extensional stiffness, $A = \sum_{i=1}^{q} Y_i b_i (z_i - z_{i-1})$
D	bending stiffness, $D = \sum_{i=1}^{q} \frac{1}{3} Y_i b_i (z_i^3 - z_{i-1}^3)$
E_3	electric field, E_3, = $V/(z_i - z_{i-1})$.
F_{tot}	force applied to entire array
F_y	force applied to one series ($F_y = F_{tot}/m$)
$[L]$	coordinate transformation matrix
M	moment
M^P	piezoelectric moment, $M^P = \sum_{i=1}^{q} \frac{1}{2} Y_i b_i (z_i^2 - z_{i-1}^2)(d_{31} E_3)$
N	normal force, $N^P = \sum_{i=1}^{q} Y_i b_i (z_i - z_{i-1})(d_{31} E_3)$
N^P	piezoelectric normal force,
R_n	neutral axis

$[T]$	tip mass matrix
U	circumferential or bending orthogonality constant
$[U_i]$	C-block transfer matrix
V	shear
V	voltage
W	radial or extensional orthogonality constant
Y	Young's modulus
γ	damping coefficient
λ_i	ith nondimensional natural frequency, $\lambda_i^2 = \frac{\rho\omega_i^2 R_n^2}{D}$
λ_{beq}	nondimensional bending natural frequency for equivalent bender, $\lambda_{beq} = (2\pi n^2)\lambda_i$
λ_{eeq}	nondimensional extensional natural frequency for equivalent bender, $\lambda_{eeq} = \left(\frac{n\pi}{\sqrt{2}}\right)\lambda_i$
φ	slope, $\varphi = (u - w_{,\theta})$
μ	ratio of the tip mass to the total mass of the C-block array
θ	angular variable measured from base of individual C-block
ρ	mass per length,
χ	nondimensional stiffness ratio, $\chi = D/AR_n^2$
ω_i	ith natural frequency
Λ	nondimensional forcing frequency, $\Lambda^2 = \frac{\rho\Omega^2 R_n^2}{D}$
Ω	forcing frequency
° pp	degrees peak-to-peak

9.2 Additional Figures

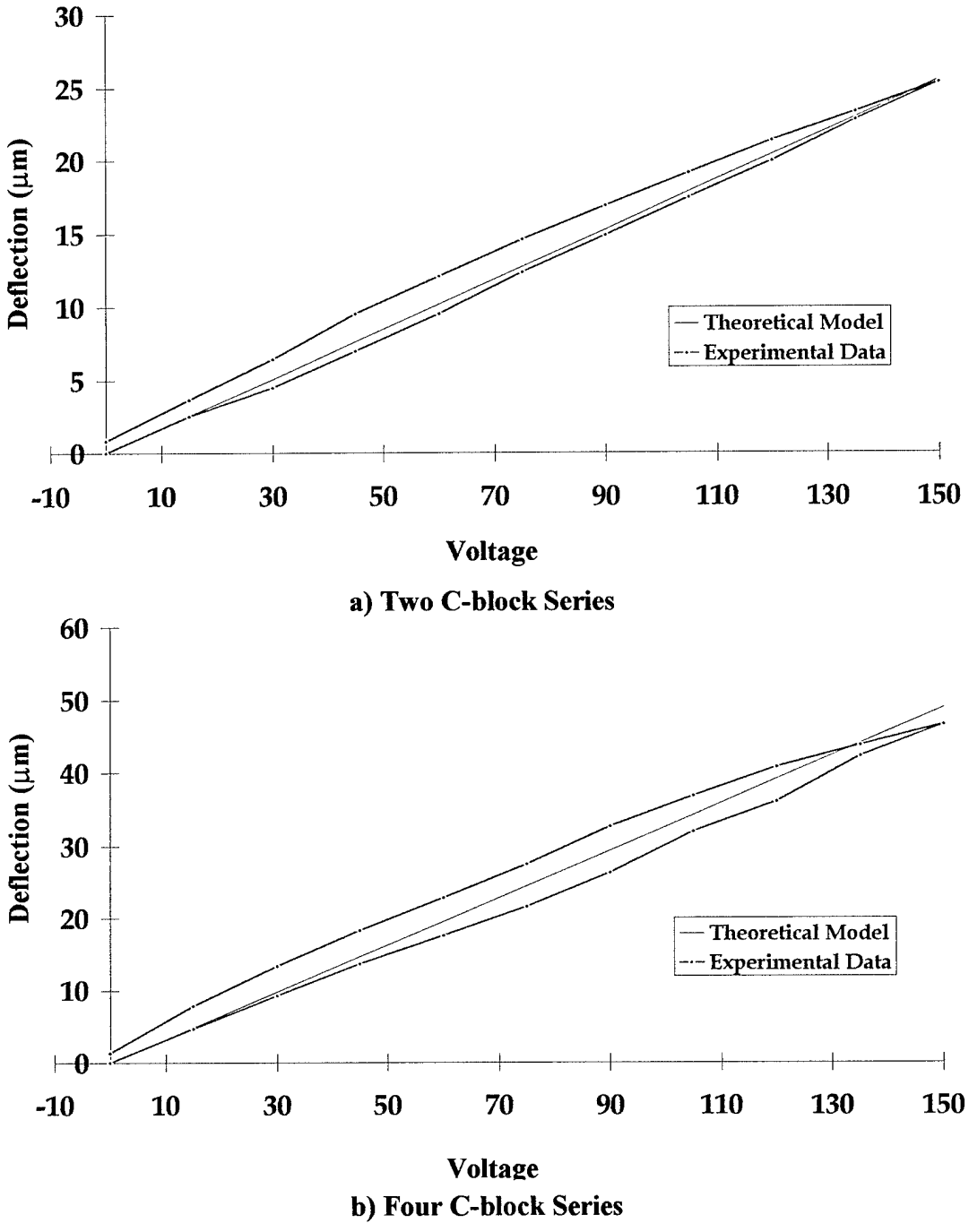

Figure 6. Deflection-Voltage Experimental Results for C-Block Array Prototypes **a)** Prototype 1: Ceramic unimorph of two C-blocks with outside radius = 10.00 mm. **b)** Prototype 2: Ceramic unimorph of four C-blocks with outside radius = 10.00 mm.

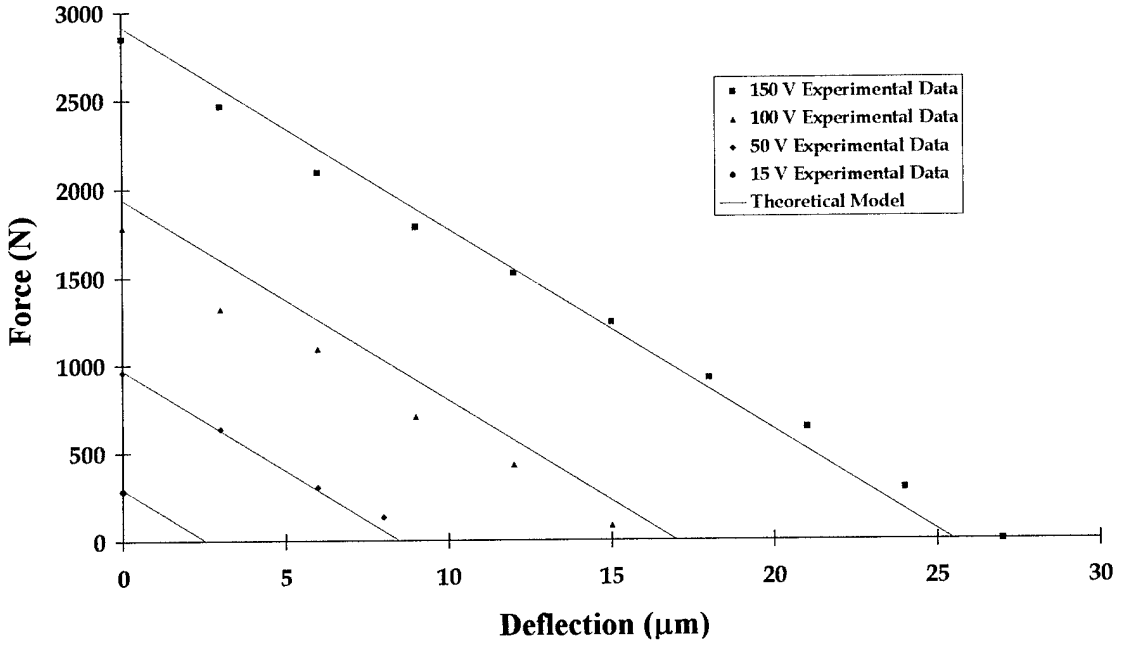

a) Two C-block Series

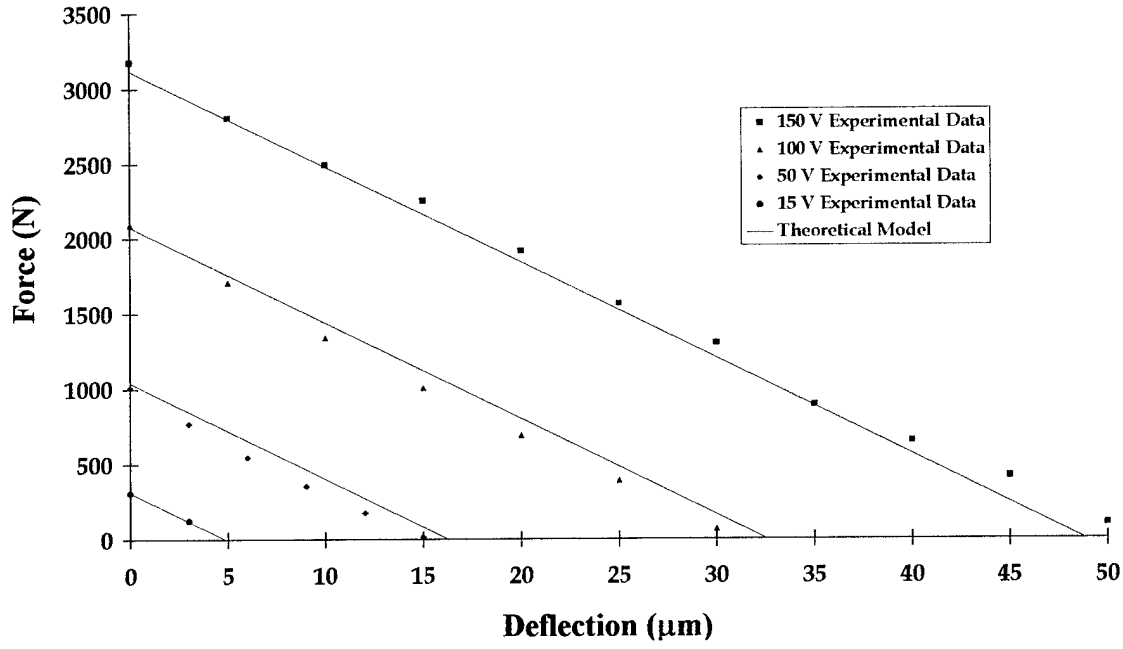

a) Four C-block Series

Figure 7. Force-Deflection Experimental Results for C-Block Array Prototypes **a)** Prototype 1: Ceramic unimorph of two C-blocks with outside radius = 10.00 mm. **b)** Prototype 2: Ceramic unimorph of four C-blocks with outside radius = 10.00 mm.

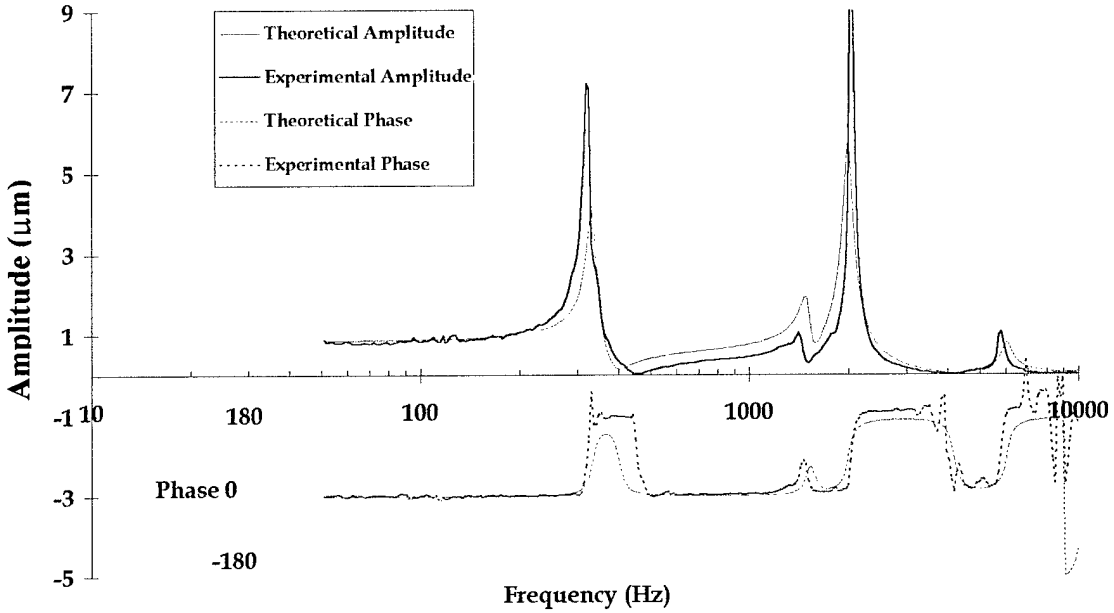

a) Two C-block series, No Tip Mass, 5 V

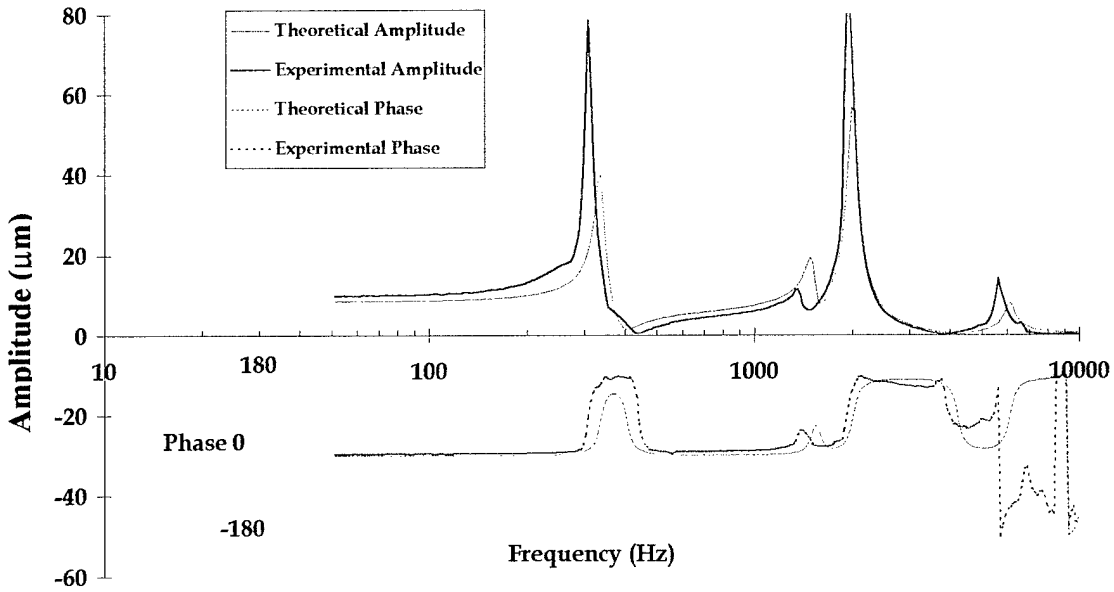

b) Two C-block series, No Tip Mass, 50 V

Figure 8. Frequency-Amplitude Experimental Results for C-Block Array Prototype 1 These results are for a ceramic unimorph of two C-blocks with outside radius = 10.00 mm with no tip mass. **a)** 5V input **b)** 50 V input.

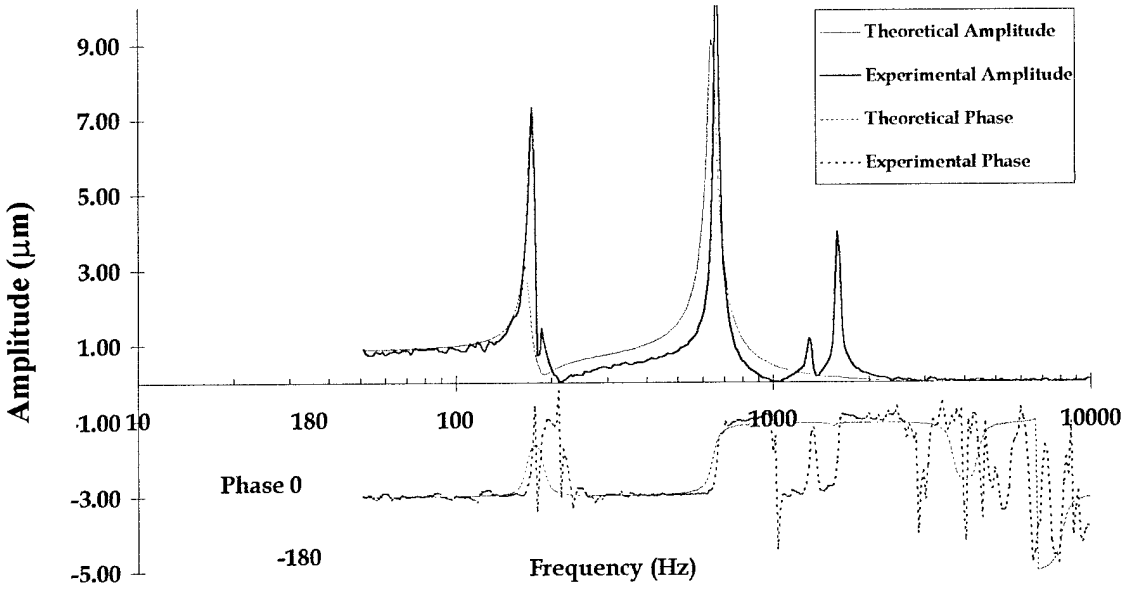

a) Two C-block series, With Tip Mass, 5 V

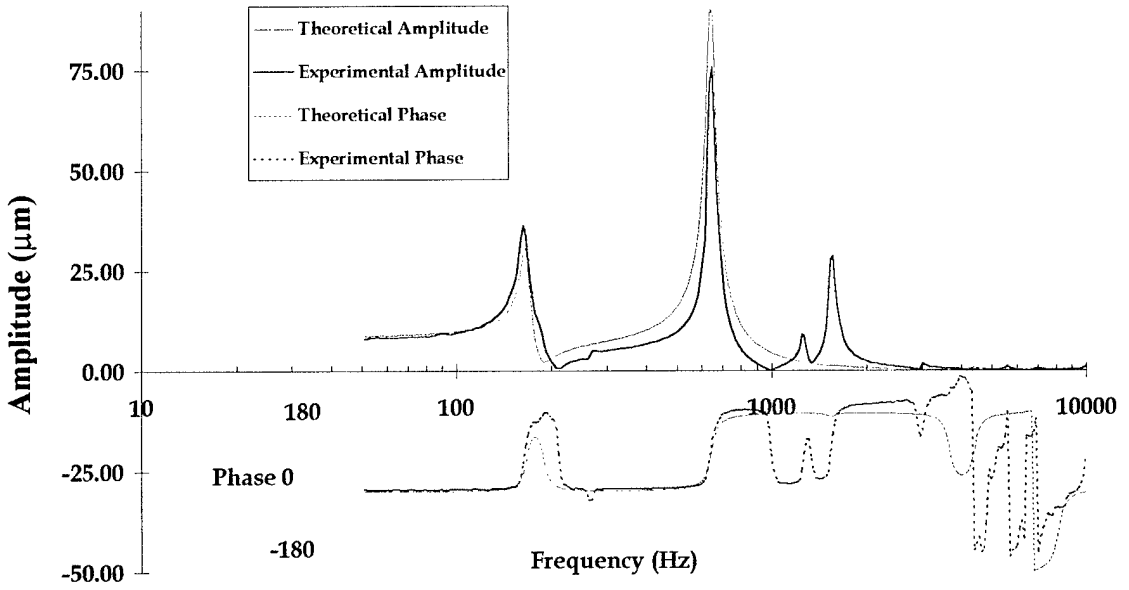

b) Two C-block series, With Tip Mass, 50 V

Figure 8. Frequency-Amplitude Experimental Results for C-Block Array Prototype 1 These results are for a ceramic unimorph of two C-blocks with outside radius = 10.00 mm with tip mass. **a)** 5V input **b)** 50 V input.

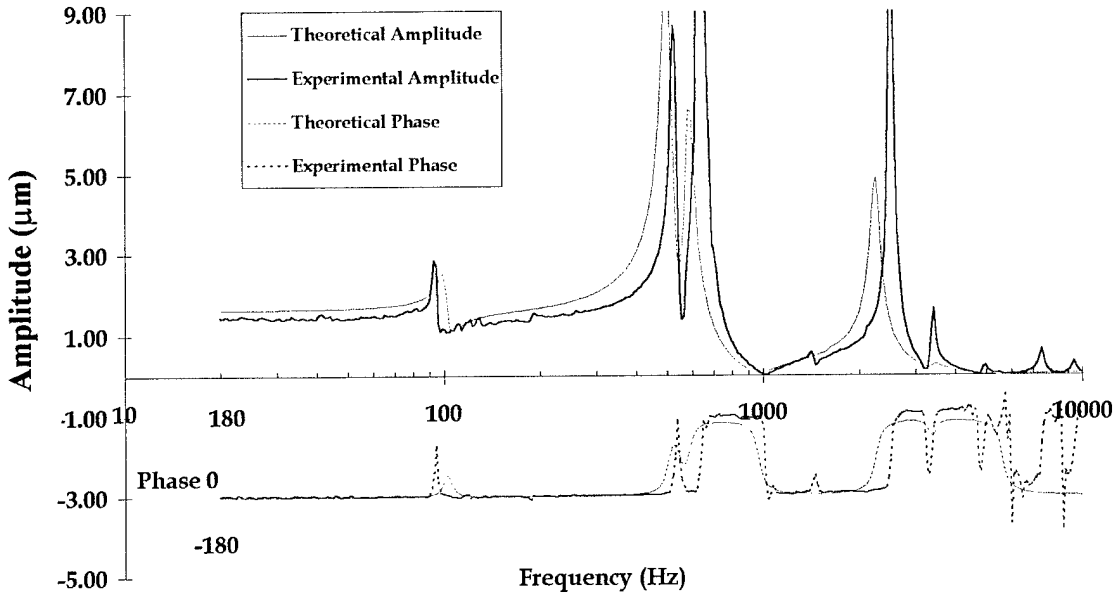

a) Four C-block series, No Tip Mass, 5 V

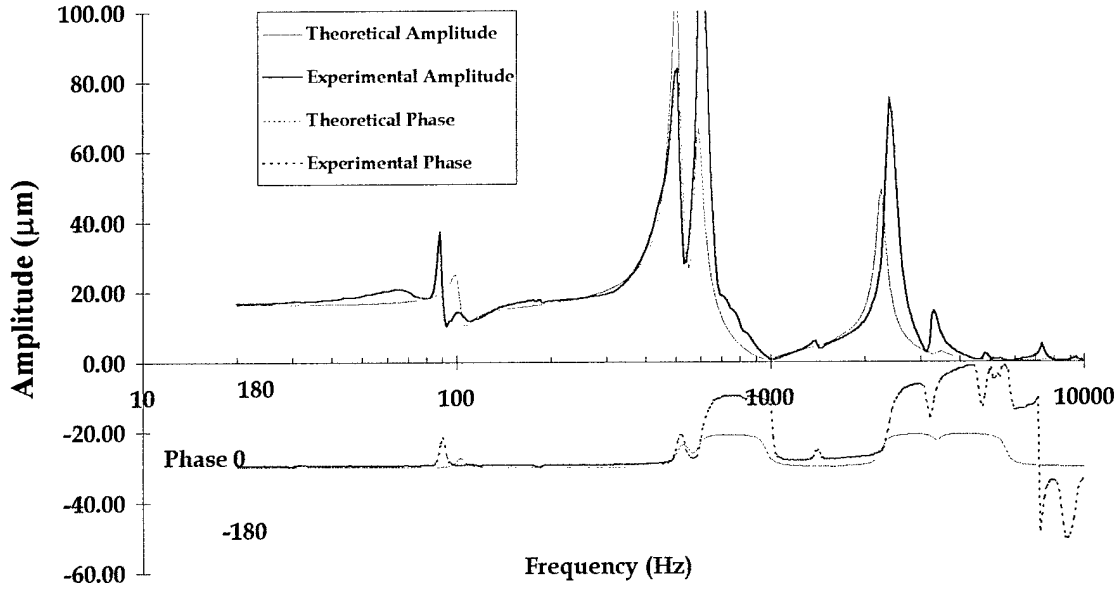

b) Four C-block series, No Tip Mass, 50 V

Figure 8. Frequency-Amplitude Experimental Results for C-Block Array Prototype 2 These results are for a ceramic unimorph of four C-blocks with outside radius = 10.00 mm with no tip mass. **a)** 5V input **b)** 50 V input.

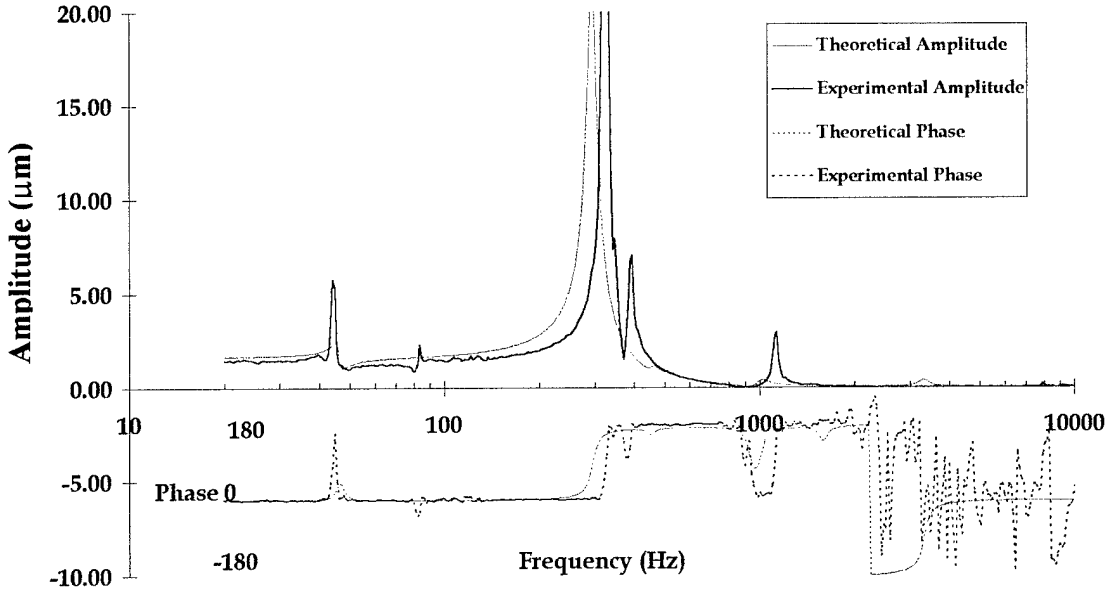

a) Four C-block series, With Tip Mass, 5 V

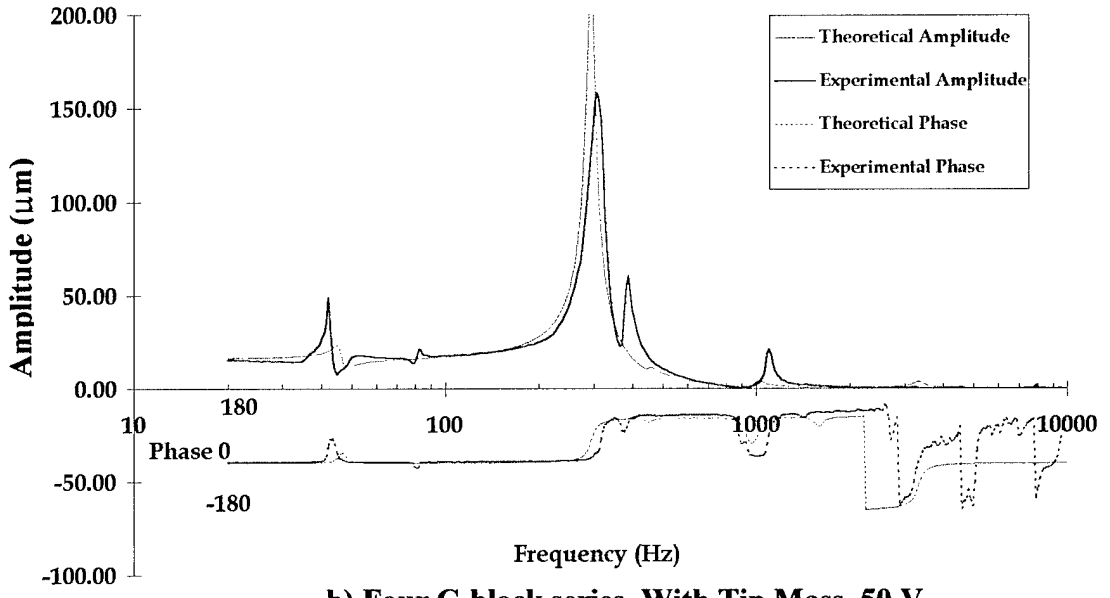

b) Four C-block series, With Tip Mass, 50 V

Figure 8. Frequency-Amplitude Experimental Results for C-Block Array Prototype 2 These results are for a ceramic unimorph of four C-blocks with outside radius = 10.00 mm with tip mass. **a)** 5V input **b)** 50 V input.

9.3 Tables

Table 1. 2^3 Factorial Experimental Results for Static C-Block Performance Effects demonstrated by the nondimensional analysis. The tip displacement is given in nondimensional microstrain. The effect and sum of squares for each nondimensional factor, number in series (s), nondimensional force (f), and nondimensional moment effectiveness (voltage or v) is shown, as well as for each combination thereof. The symbols "+" and "-" indicate the appropriate sign used in combining the strain.

		Factors							
Test	μstrain	total	s	v	f	s-v	s-f	v-f	s-v-f
1	12.53	+	+	+	+	+	+	+	+
2	640.8	+	+	+	-	+	-	-	-
3	-0.309	+	+	-	+	-	+	-	-
4	64.21	+	+	-	-	-	-	+	+
5	-16.55	+	-	+	+	-	-	+	-
6	694.0	+	-	+	-	-	+	-	+
7	-2.152	+	-	-	+	+	-	-	+
8	69.40	+	-	-	-	+	+	+	-
Effects		365.5	-6.870	299.9	-368.7	-5.198	22.33	-300.7	18.82
Sum Squares		634400	94.39	179900	271900	54.05	997.6	180800	708.4

Table 2. 2^4 Factorial Experiment Results for Dynamic C-Block Performance Effects demonstrated by the nondimensional analysis. The tip displacement is given in nondimensional microstrain. The effect of each nondimensional factor, number in series, nondimensional moment effectiveness (voltage), nondimensional frequency, and nondimensional tip mass is shown, as well as the sum of squares. The symbols "+" and "-" indicate the appropriate sign used in combining the strain.

		Factors							
Test	μstrain	total	s	v	ω	m	s-ω	s-v	v-ω
1	243.8	+	+	+	+	+	+	+	+
2	239.8	+	+	+	+	-	+	+	+
3	214.0	+	+	+	-	+	-	+	-
4	230.6	+	+	+	-	-	-	+	-
5	19.26	+	+	-	+	+	+	-	-
6	20.55	+	+	-	+	-	+	-	-
7	19.36	+	+	-	-	+	-	-	+
8	19.86	+	+	-	-	-	-	-	+
9	181.0	+	-	+	+	+	-	-	+
10	162.2	+	-	+	+	-	-	-	+
11	218.4	+	-	+	-	+	+	-	-
12	270.9	+	-	+	-	-	+	-	-
13	15.60	+	-	-	+	+	-	+	-
14	12.00	+	-	-	+	-	-	+	-
15	24.82	+	-	-	-	+	+	+	+
16	23.89	+	-	-	-	-	+	+	+
Effects		239.5	12.29	200.7	-15.94	-5.446	25.86	11.61	-10.81
Sum Squares		169700	604.6	161100	1017	118.6	2674	539.4	467.9

		Factors							
Test	μstrain	s-m	ω-m	v-m	s-v-ω	s-ω-m	s-v-m	v-ω-m	s-v-ω-m
1	243.8	+	+	+	+	+	+	+	+
2	239.8	-	-	-	+	-	-	-	-
3	214.0	+	-	+	-	-	+	-	-
4	230.6	-	+	-	-	+	-	+	+
5	19.26	+	+	-	-	+	+	-	-
6	20.55	-	-	+	-	-	-	+	+
7	19.36	+	-	-	+	-	+	+	+
8	19.86	-	+	+	+	+	-	-	-
9	181.0	-	+	+	-	-	-	+	-
10	162.2	+	-	-	-	+	+	-	+
11	218.4	-	-	+	+	+	-	-	+
12	270.9	+	+	-	+	-	+	+	-
13	15.60	-	+	-	+	-	+	-	+
14	12.00	+	-	+	+	+	-	+	-
15	24.82	-	-	-	-	+	+	+	-
16	23.89	+	+	+	-	-	-	-	+
Effects		1.855	11.71	-6.132	20.43	-6.766	3.438	11.24	-5.898
Sum Squares		13.76	548.3	150.4	1670	183.1	47.28	505.0	139.2

Table 3. C-Block Array Deflection-Voltage Experimental Results The maximum input voltage and corresponding nondimensional moment effectiveness (Eq. 7.6) are given for both prototypes. In addition, the maximum deflection and corresponding strain (Eq. 7.5) are given, along with the mean difference between the theoretically predicted displacement and the experimental results.

Proto	No. in Series	Max. Voltage	Max Nondim Moment	Max. Defl. (μm)	Max. Microstrain	Mean Diff, Theory to Expt. (μm)	%
1	2	150	700 E-6	25.3	694	0.813	3.19%
2	4	150	673 E-6	46.5	641	2.13	4.36%

Table 4. C-Block Array Force-Deflection Experimental Results The maximum (blocked) force and nondimensional force (Eq. 7.7) that was experimentally measured is given for both prototypes at three input voltages. The corresponding nondimensional moment effectiveness (Eq. 7.6) is also given, as well as the mean difference between the theoretically predicted force and the experimental results.

Proto.	No. in Series	Input Voltage	Nondim. Moment	Max Force (mN)	Nondim. Max. Force	Mean Diff: Theory to Expt. (mN)	%
1	2	50	233 E-6	972	231E-6	23.6	0.833%
		100	467 E-6	1940	428 E-6	178.4	6.27%
		150	700 E-6	2920	683 E-6	96.4	3.39%
2	4	50	224 E-6	1039	219 E-6	80.7	2.54%
		100	449 E-6	2080	452 E-6	89.5	2.82%
		150	673 E-6	3180	685 E-6	84.2	2.65%

Table 5. C-Block Array Frequency-Amplitude Experimental Results The experimentally determined locations of the natural frequencies, and the nondimensional values of these frequencies (Eq. 5.40) are given for both prototypes. Each prototype was tested four times: at 5V with and without a tip mass, and at 50V with and without a tip mass.

Proto	μ Tip Mass	5V Input Testing				50V Input Testing			
		Static Defl (μm)	Mode	Exper Natural Freq (Hz)	Nondim. Freq. Location	Static Defl (μm)	Mode	Exper Natural Freq (Hz)	Nondim. Freq. Location
1	0	0.86	1	322	0.1133	9.87	1	311	0.1269
			2	1410	0.575		2	1350	0.551
			3	2044	0.834		3	1958	0.799
			4	5761	2.35		4	5650	2.30
			5	----	----		5	9263	3.78
1	1	0.88	1	171	0.0697	7.95	1	163	0.665
			2	665	0.271		2	642	0.262
			3	1600	0.653		3	1550	0.632
2	0	1.44	1	94	0.0315	16.75	1	89	0.0298
			2	525	0.1758		2	502	0.1680
			3	644	0.216		3	604	0.202
			4	1412	0.473		4	1390	0.465
			5	2509	0.840		5	2410	0.807
			6	3400	1.138		6	3318	1.111
2	1	1.42	1	44.5	0.01500	15.60	1	42	0.01406
			2	327	0.1095		2	308	0.1031
			3	393	0.1315		3	389	0.1302
			4	1125	0.377		4	1101	0.369

Table 6. Error for C-Block Array Frequency-Amplitude Experimental Results The average difference between the analytical model and the experimental results are given for the tip deflection and natural frequency locations. The percentage difference between the experimental value and analytical prediction is also given.

Proto	μ Tip Mass	Deflect: Av. Diff Thry to Exp (μm)	Deflect: % Diff Thry to Expmnt.	Mode	Exp Freq Location at 5 V (Hz)	% Diff. from Theory to Exp	Exp Freq Location at 50 V (Hz)	% Diff. from Theory tc Exp.
1	0	at 5V: 0.306 at 50V: 3.08	at 5V: 3.02 at 50V: 3.55	1	322	-3.24%	311	-7.42%
				2	1410	-5.71%	1350	-10.53%
				3	2044	2.91%	1958	-2.37%
				4	5761	4.46%	5650	-7.19%
				5	----	----	9263	-8.11%
1	1	at 5V: 0.418 at 50V: 3.04	at 5V: 3.91 at 50V: 4.03	1	171	2.84%	163	-1.97%
				2	665	3.68%	642	0.17%
				3	1600	3.74%	1550	0.54%
					----	----	----	----
2	0	at 5V: 0.745 at 50V: 4.24	at 5V: 3.21 at 50V: 3.26	1	94	-6.72%	89	-11.98%
				2	525	4.72%	502	-0.11%
				3	644	10.31%	604	3.11%
				4	1412	-11.16%	1390	-12.85%
				5	2509	12.03%	2410	7.24%
				6	3400	-0.22%	3318	-2.96%
2	1	at 5V: 0.856 at 50V: 4.16	at 5V: 1.87 at 50V: 2.64	1	44.5	-3.12%	42	-8.57%
				2	327	11.22%	308	4.76%
				3	393	-13.15%	389	-14.03%
				4	1125	11.65%	1101	9.27%